Multi-model evaluation of short-lived pollutant distributions over East Asia during summer 2008

Boris Quennehen, Jean-Christophe Raut, Kathy S. Law, Gérard Ancellet, Cathy Clerbaux, S.-W. Kim, M. T. Lund, G. Myhre, D. J. L. Olivié, Sarah Safieddine, et al.

Atmos. Chem. Phys. Discuss., 15, 11049–11109, 2015
www.atmos-chem-phys-discuss.net/15/11049/2015/
doi:10.5194/acpd-15-11049-2015

Atmospheric Chemistry and Physics Discussions

Multi-model evaluation of short-lived pollutant distributions over East Asia during summer 2008

B. Quennehen[1,*], J.-C. Raut[1], K. S. Law[1], G. Ancellet[1], C. Clerbaux[1], S.-W. Kim[2], M. T. Lund[3], G. Myhre[3], D. J. L. Olivié[4], S. Safieddine[1], R. B. Skeie[3], J. L. Thomas[1], S. Tsyro[4], A. Bazureau[1], N. Bellouin[5], N. Daskalakis[6,7], M. Hu[8], M. Kanakidou[6], Z. Klimont[9], K. Kupiainen[9], S. Myriokefalitakis[6,7], J. Quaas[10], S. T. Rumbold[11,], M. Schulz[4], R. Cherian[10], A. Shimizu[12], J. Wang[8], S.-C. Yoon[2], and T. Zhu[8]**

[1]Sorbonne Universités, UPMC Univ. Paris 06, Université Versailles St-Quentin, CNRS/INSU, LATMOS-IPSL, Paris, France
[2]School of Earth and Environmental Sciences, Seoul National University, Seoul, Korea
[3]Center for International Climate and Environmental Research – Oslo (CICERO), Oslo, Norway
[4]Norwegian Meteorological Institute, Oslo, Norway
[5]Department of Meteorology, University of Reading, Reading, RG6 6BB, UK
[6]Environmental Chemical Processes Laboratory, Department of Chemistry, University of Crete, Heraklion, Crete, Greece

[7]Institute of Chemical Engineering Sciences (ICE-HT), FORTH, Patra, Greece
[8]College of Environmental Sciences and Engineering, Peking University, Beijing, China
[9]International Institute for Applied Systems Analysis (IIASA), Laxenburg, Austria
[10]Institute for Meteorology, Universität Leipzig, Leipzig, Germany
[11]Met Office Hadley Centre, Exeter, EX1 3PB, UK
[12]National Institute for Environmental Studies, Ibaraki, Japan
[*]now at: Univ. Grenoble Alpes/CNRS, Laboratoire de Glaciologie et Géophysique de l'Environnement (LGGE), 38041 Grenoble, France
[**]now at: NCAS-Climate, University of Reading, Reading, RG6 6BB, UK

Received: 5 February 2015 – Accepted: 26 March 2015 – Published: 15 April 2015

Correspondence to: B. Quennehen (quennehen@latmos.ipsl.fr)

Published by Copernicus Publications on behalf of the European Geosciences Union.

ACPD
15, 11049–11109, 2015

Abstract

The ability of six global and one regional model to reproduce distributions of tropospheric ozone and its precursors, as well as aerosols over Asia in summer 2008 is evaluated using satellite and in-situ observations. Whilst ozone precursors (NO_2 and CO) are generally underestimated by the models in the troposphere, surface NO_2 concentrations are overestimated, suggesting that emissions of NO_x are too high. Ozone integrated columns and vertical profiles are generally well modeled, but the global models face difficulties simulating the ozone gradient at the surface between urban and rural environments, pointing to the need to increase model resolution. The accuracy of simulated aerosol patterns over eastern China and northern India varies between the models, and although most of the models reproduce the observed pollution features over eastern China, significant biases are noted in the magnitude of optical properties (aerosol optical depth, aerosol backscatter). These results have important implications for accurate prediction of pollution episodes affecting air quality and the radiative effects of these short-lived climate pollutants over Asia.

1 Introduction

Short-lived pollutants (SLPs), defined here as tropospheric ozone and aerosols including black carbon (BC) were recently the focus of several important efforts by the scientific community due to their potential role in emerging strategies aiming to mitigate global climate change and improve air quality (Shindell et al., 2012; Anenberg et al., 2012). Due to their relatively short lifetimes (e.g., aerosol lifetime in the troposphere is about one week Pruppacher and Klett, 1978), the impact of SLP (as well as ozone precursors) emission reductions on near-term reductions in the rate of climate warming has been examined in several recent studies (Ramanathan and Carmichael, 2008; Jackson, 2009; Penner et al., 2010; Shoemaker et al., 2013; Smith and Mizrahi, 2013; Rogelj et al., 2014). In particular, due to recent fast increases in SLP and ozone

ACPD
15, 11049–11109, 2015

precursor emissions (Streets et al., 2003; Richter et al., 2005; Klimont et al., 2013; Wang et al., 2014; Klimont et al., 2015), East Asia is a key region being targeted by mitigation strategies. This region is already highly polluted with elevated near surface pollutant concentrations, especially over eastern China (Wang et al., 2011; Yang et al., 2011), producing severe environmental impacts (Ma et al., 2010). Shao et al. (2006) presented observations from 360 cities in China showing that the national ambient air quality limits were exceeded in 70 % of the cases. More specifically, three areas in eastern China are shown, by several studies, to be major polluted regions (Chan and Yao, 2008; Ma et al., 2012; Boynard et al., 2014): the North China Plain (NCP, which includes Beijing and Tianjin), the Yangtze river delta (YRD, which includes Shanghai), and the Pearl river delta (PRD, which includes Honk-Kong and Guangzhou). It is therefore important to assess the source of this regional pollution and to evaluate the ability of chemistry-aerosol-climate models to simulate the distributions of SLPs over this region.

Ozone is a reactive species impacting both climate and air quality. In the troposphere, it is produced photochemically from the oxidation of carbon monoxide (CO), methane, non-methane volatile organic compounds (VOCs) by OH radicals in the presence of nitrogen oxides (NO_x). It also has natural sources such as the flux from the stratosphere. Due to photochemical loss, it has a lifetime in the troposphere of a few weeks (Stevenson et al., 2006). It is also removed by dry deposition to the surface. Radiative forcing due to tropospheric ozone over industrial era is estimated to be $0.40 \pm 0.20\,\mathrm{W\,m^{-2}}$ (Myhre et al., 2013). Tropospheric ozone pollution over the three most polluted Chinese regions is influenced by the Asian summer monsoon (Liu et al., 2002; Xu et al., 2008; Lin et al., 2009; He et al., 2008; Safieddine et al., 2013) and regional photochemical pollution (Lin et al., 2008). Long-term time series of ozone measurements were reported for Hong-Kong (T. Wang et al., 2009) and Beijing (Ding et al., 2008), showing increasing background concentrations at both locations, whereas seasonal and day-to-day variations over the NCP, YRD, and PRD regions in 2008 were studied by Dufour et al. (2010) using satellite observations. A seasonal maximum is

ACPD
15, 11049–11109, 2015

found over East Asia in late spring due to increased solar radiation whereas a minimum is found in summer for the PRD and YRD, and in winter for the NCP (Naja and Akimoto, 2004; Li et al., 2007; He et al., 2008; Safieddine et al., 2013). The main mechanism driving the summer minimum is the intrusion of low-ozone marine air masses coming from the tropical Pacific ocean, i.e., the monsoon (Lin et al., 2009).

Several regional model evaluations of trace gases have been carried out with a focus on East Asia. In the frame of the MICS-Asia phase II project, Han et al. (2008) showed good agreement between eight regional models and SO_2 observations from the TRACE-P campaign (Fuelberg et al., 2003), whereas modeled ozone accuracy varied with the region and the season. Model performance regarding NO_x was relatively poor with a systematic underestimation by all the models. A previous study by Zhang et al. (2006), comparing TRACE-P airborne observations with a regional model simulation, found similar results as Han et al. (2008) but with a more accurate reproduction of NO_x concentrations. CO concentrations were underestimated by Gao et al. (2009) at two surface stations in Japan whereas ozone seasonal variation and concentration simulated were in agreement with the observations.

Atmospheric aerosol plays a major role in the Earth's radiative balance by scattering (McCormick and Ludwig, 1967) and absorbing solar radiation (Haywood and Shine, 1995). Aerosols also affect the formation, lifetime and albedo of clouds (Albrecht, 1989; Twomey, 1977; Ackerman et al., 2000), causing indirect effects on the radiative balance. According to recent estimates, atmospheric aerosols, emitted by anthropogenic and natural sources (e.g., heating, transportation, biomass burning and dust), have, since pre-industrial times, modified the aerosol direct effect by $-0.35 \pm 0.50\,W\,m^{-2}$ (Myhre et al., 2013) whereas the total (direct and indirect) effects modified the Earth's radiative balance by $-1.3 \pm 0.4\,W\,m^{-2}$ (Cherian et al., 2014). Radiative forcing due to absorbing species (e.g., BC) at the top-of-atmosphere is shown to be positive (Haywood and Shine, 1995). BC is the carbonaceous component of soot, resulting from incomplete combustion. In a recent extensive study, Bond et al. (2013) estimated the BC direct radiative forcing for the industrial era to be $0.51\,W\,m^{-2}$ whereas

ACPD
15, 11049–11109, 2015

Myhre et al. (2013) reported a forcing of 0.40 W m^{-2} (0.05–0.80). 90 % of BC emissions are due to diesel engines, industry, residential burning, and open burning (Bond et al., 2013). Aerosol impacts on air quality are also a serious problem since aerosols reduce visibility (sometimes dramatically, e.g., Zhao et al., 2011; Chen et al., 2012; Li et al., 2013) and cause, together with ozone, serious health deterioration and premature deaths (Nawahda et al., 2012).

Many studies have discussed observations of aerosol properties over East Asia (e.g., Kim et al., 2007) and, more specifically, over the three regions mentioned above. A clear seasonal cycle is observed for organic carbon (OC) and BC with maximum and minimum concentrations in winter and summer, respectively (Cao et al., 2004; Sun et al., 2004; Yang et al., 2005; Huang et al., 2006).

The ability of global models to simulate monthly aerosol optical depths (AODs) was examined by Kinne et al. (2006) over East Asia in summer with comparisons showing important underestimation of observed AODs. Kinne et al. (2006) also pointed out that uncertainties in the direct radiative forcing could be larger than differences in AOD suggest. The aerosol vertical distribution was investigated by Koffi et al. (2012) who compared global model results with aerosol extinction mean profiles from satellite observations over specific regions, including East Asia. They found generally good agreement in the vertical shape of extinction profiles between the models and the observations. However, accuracy depended highly on the model, season and region. Large discrepancies in modeled surface BC concentrations compared to observations were reported by Koch et al. (2009) whereas Samset et al. (2013) and Allen and Landuyt (2014) concluded that BC vertical distributions are a major source of uncertainty in BC radiative forcing estimations.

In this context, the European Union (EU) Evaluating the CLimate and air quality ImPacts of Short-livEd pollutants (ECLIPSE) project was launched with the objective to develop and assess effective emission abatement strategies in order to provide sound scientific advice about measures to mitigate climate change and improve air quality. ECLIPSE models versions are more recent than those evaluated in the cited evaluation

ACPD
15, 11049–11109, 2015

studies, thus one focus of the project is the evaluation of global and regional chemical-aerosol-climate models over two important emission regions (Europe and Asia) and one receptor region (the Arctic). The aim of this paper is to evaluate the performance of six global and one regional model, run using the same ECLIPSE emission dataset, by comparison against observations over East Asia. Diagnoses used in this study allow to control the driving processes affecting both air quality (e.g., surface concentration) and climate (e.g., vertical profiles of optical properties). The East asia region is a focus because, as noted above, it is a region with high pollution levels where emissions still appear to be increasing but where mitigation options are also being actively considered. East Asian emissions originate from several different sources including anthropogenic emissions, biomass burning, and dust episodes. In addition, pollution from Asia can be transported many thousand kilometers downwind to North America (e.g., Jaffe et al., 1999) as well as to the Arctic (e.g., Roiger et al., 2011). The focus of this study is on summer (August and September) 2008; a period for which the intensive observations from the CAREBEIJING 2008 measurement campaign (Huang et al., 2010; Zhang et al., 2014) are available. The CAREBEIJING 2008 campaign took place in August and September 2008 in the context of the Beijing Olympic and Paralympic games. SLPs emissions mitigation was attempted between 30 June to 20 September 2008 (see the detailed mitigation plan in Wang et al., 2010) and concerned polluting vehicles, as well as the chemical and power plants within the Beijing province. The impacts of this pollutant emission mitigation have been reported in several studies. Wang and Xie (2009) and Zhou et al. (2010) observed reduction of 19 to 57 % in CO and 28 to 52 % in PM_{10} on-road emissions, whereas Y. Wang et al. (2009) reported decrease of 21 % in summer 2008 CO observation compared to 2006 and 2007 at a remote site 100 km away from Beijing and concluded, based on a model analysis, that ozone concentrations were reduced by 2–10 ppbv over the NCP region during the mitigation period. At a larger scale, Worden et al. (2012) used satellite observations to deduce a 11 % reduction in CO emissions over Beijing. Although lower pollutant concentrations can be observed, particularly in the south and in coastal regions due to the monsoon influ-

ACPD
15, 11049–11109, 2015

ences at this time of year (Kim et al., 2007), high pollution episodes still occur (Flowers et al., 2010). Improved estimation of the radiative impact of SLPs requires careful evaluation of model performance, in particular with respect to the vertical distribution of ozone, aerosols and their precursors. This study focuses on evaluating models at the surface and in the free troposphere, where pollutant distributions are important for air quality and climate, respectively.

The models used in this study and datasets used to assess model performance are described in Sect. 2 as well as the meteorological situation during summer 2008. Evaluation of simulated trace gas distributions on different temporal and spatial scales are presented in Sect. 3. Comparisons between observed and modeled aerosol optical properties as well as available surface/aircraft data on aerosol chemical composition, are discussed in Sect. 4. The summary and conclusions are given in Sect. 5.

2 Models, evaluation datasets and meteorological conditions

In this section, the global and regional models involved in this study are presented together with the different measurement datasets used to evaluate their performance including satellite data, ground-based, and airborne measurements. The meteorological conditions over East Asia during summer 2008 are also briefly described.

2.1 Models description

The main model characteristics are listed in Table 1. Within the ECLIPSE project, a dedicated anthropogenic emission dataset was developed (ECLIPSE V4, Klimont et al., 2015). Whilst ECLIPSE emissions are annual averages for most of the sectors, a seasonal cycle is applied to the domestic sector (Streets et al., 2003). In addition, agricultural waste burning fires are included in the inventory. Emission reductions associated with the mitigation strategies during the Olympic period mentioned in the Introduction are not taken into account in the ECLIPSE anthropogenic emis-

ACPD
15, 11049–11109, 2015

sions. Wildfire emissions were taken from GFED 3.1 (van der Werf et al., 2010) and aircraft/shipping emissions were from the RCP 6.0 scenario (Lee et al., 2009; Buhaug et al., 2009), respectively) whereas biogenic emissions were prescribed individually by each model (see Table 1). Dust, sea salt and DMS emissions were also model-dependent. WRF-Chem provides online dust and sea-salt emissions but only the latter are used in the ECLIPSE simulations due to an overestimation of dust loads, as reported by Saide et al. (2012). The main dust sources in East Asia are located in dry regions of China and Mongolia, north of the Himalayas (Taklamakan, Gobi and Gurbantunggut deserts). Most of the dust events occur in spring (Huang et al., 2013) whilst in summer, due to the Asian summer monsoon flux, rather little dust is transported to coastal areas (Kim et al., 2007). Thus, neglecting this source in WRF-Chem summertime simulations is not expected to introduce large bias in the aerosol loads. Global model simulations were conducted for 2008 with a one or two years spin-up (depending on the model) whereas the regional WRF-Chem simulation was for August and September 2008 with a 10 day spin-up using initial chemical and boundary conditions from the Mozart model.

2.2 Satellite observations

Several satellite datasets have been used in this evaluation since they provide useful information about the spatial distribution of pollutants and their precursors. The Infrared Atmospheric Sounding Interferometer (IASI) sensor mounted onboard the MetOp-A platform has provided data since June 2007. It is a nadir-looking Fourier transform spectrometer working in the thermal infrared spectral range (645–2760 cm^{-1}) (Clerbaux et al., 2009). It can detect several trace gases including ozone and CO. The MetOp-A orbit is sun-synchronous and provides complete observation of the Earth' surface every day. However, clouds may affect the signal and lead to errors in the retrieved data. The software used for the retrieval of the ozone global distribution is the Fast Optimal Retrievals on Layers for IASI (FORLI-O3, Hurtmans et al., 2012).

ACPD
15, 11049–11109, 2015

The second Global Ozone Monitoring Experiment (GOME-2, Munro et al., 2000), also onboard the Metop-A satellite, is a nadir-looking spectrometer covering the spectral range between 240 and 790 nm at 0.2–0.4 nm resolution. With its large swath of 1920 km, GOME-2 provides near global daily coverage. The GOME-2 sensor uses the Differential Optical Absorption Spectroscopy (DOAS) technique to observe the atmosphere and tropospheric NO_2 concentrations are retrieved using the algorithm developed by Boersma et al. (2004).

AOD space-borne observations are collected by the Moderate resolution Imaging Spectrometer (MODIS) instrument onboard 2 satellites, Aqua and Terra, flying opposing orbits, providing global coverage of the Earth every 1–2 days. The MODIS level 3 products used in this study are described by Hubanks et al. (2008).

Vertical distributions of aerosols and clouds are probed with the Cloud-Aerosol LIdar with orthogonal Polarisation (CALIOP) instrument mounted on the CALIPSO satellite, part of the A-train satellite constellation. CALIOP is a two wavelength (532 and 1064 nm) polarisation-sensitive lidar as described by Winker et al. (2007).

2.3 Ground-based data

The locations of the measurement stations used in this study are shown in Fig. 1, whereas the station coordinates are given in Table 2. During the CAREBEIJING 2008 campaign, SLP concentrations were measured at the air quality observatory of Peking University (PKU) in Beijing which can be considered as a typical urban environment. Instrumentation deployed at the observatory measured ozone, NO_x (defined as the sum of NO and NO_2), and CO (Chou et al., 2011), as well as PMs ($PM_{2.5}$ and PM_{10}), OC and BC (Huang et al., 2010).

The Gosan observatory (Kim et al., 2005) is a long-term observatory located on the Jeju island, South Korea, measuring OC, BC, aerosol number size distributions (Flowers et al., 2010), and NO_x, SO_2, CO and ozone concentrations. It is not influenced by local pollutant emissions and experiences continental dust and/or pollution outflow from continental Asia (e.g., Kim et al., 2005).

ACPD
15, 11049–11109, 2015

Aerosol backscatter signals measured by the Japanese National Institute for Environmental Studies (NIES) ground-based lidar network (Shimizu et al., 2004; Sugimoto et al., 2008) are also used to evaluate model results. The spatial resolution of this network covers Japan with 10 lidars calibrated using a similar procedure. Backscatter data are available on-line on a hourly basis, allowing a robust validation of the models.

2.4 Airborne dataset

As part of the CAREBEIJING 2008 campaign, 12 scientific flights were performed over the area south of Beijing in the Hebei province. Flights followed linear routes at altitudes in the range 500–2100 m in order to sample both the boundary layer and the free troposphere. The instrumentation on board the aircraft is described by Zhang et al. (2014) and includes ozone, CO, SO_2 and NO_x samplers. The flight tracks are shown in blue in Fig. 1.

2.5 Meteorological context

During summer 2008, East Asia was mostly influenced by the Asian summer monsoon with dominant synoptic winds blowing from the south-eastern Pacific Ocean, as seen in Fig. 1. These winds transport clean marine air to the Chinese coast and thus contribute to reducing pollutant concentrations. He et al. (2008) presented seasonal distributions of ozone and the monsoon index over East Asia, showing how the impact of the monsoon decreases gradually from coastal polluted regions to inland areas and induces transport of high ozone concentrations inland. However, the monsoon also increases relative humidity in coastal regions increasing aerosol sizes and decreasing visibility. The representation of the monsoon transport varies between the models used in this study. This is illustrated in Fig. 1 which highlights the differences between the model meteorological fields, especially over the NCP region where ECMWF (European center for medium-range weather forecast) and NCEP (National centers for environmental predictions) FNL (final) fields show a lower relative humidity (RH) than NorESM. Also,

ACPD
15, 11049–11109, 2015

NorESM predicts strong winds blowing from the west over the continent in contrast to the ECMWF and NCEP analyses used to force other models. The transport of pollution is partly influenced by the meteorological parameters (e.g., winds) and differences between them can partially explain the variability in the model results.

3 Evaluation of modeled trace gas distributions

In this section, model results are first compared with the 0–20 and 0–6 km ozone columns observed by IASI, as well as NO_2 tropospheric columns detected by GOME-2. Secondly, the ability of models to simulate ozone and its precursors (NO_x and CO) reported by ground-based measurements at various Chinese and Korean stations is evaluated. Thirdly, in order to examine modeled trace gas vertical distributions, comparisons with aircraft observations from the CAREBEIJING campaign are presented.

3.1 Ozone columns

Day and night observations of IASI ozone are used to evaluate the models. Due to the variation of the IASI sensor's sensitivity with altitude, modeled ozone values need to be smoothed using the following equation:

$$\mathbf{X}_{\text{smooth}} = \mathbf{AK} \times \mathbf{X}_{\text{model}} + (\mathbf{I} - \mathbf{AK}) \times \mathbf{X}_{\text{apriori}} \quad (1)$$

where **AK** is the averaging kernels matrix, **I** is the identity matrix and $\mathbf{X}_{\text{smooth}}$, $\mathbf{X}_{\text{model}}$, and $\mathbf{X}_{\text{apriori}}$ are the smoothed, modeled, and a priori ozone profiles, respectively. **AK** and $\mathbf{X}_{\text{apriori}}$ are obtained when inverting the measured signal. The 0–20 km column is then retrieved by adding the smoothed profiles over all altitudes. **AK** is a 40 × 40 matrix, and when it is multiplied by $\mathbf{X}_{\text{model}}$, every layer has an influence on the 39 other layers. Here, the 0–20 km column is defined as the 0–20 km column thus excluding the maximum ozone concentrations in the stratosphere. Nevertheless, an overestimation of the ozone stratospheric maximum by a model could lead to an overestimation

ACPD
15, 11049–11109, 2015

in other layers. Whilst the 0–20 km columns largely reflect the ozone distribution in the lower stratosphere and give some indication about model variability in this source region for the troposphere, the 0–6 km columns are mainly influenced by lower tropospheric ozone sources (Boynard et al., 2009). It should be noted that the WRF-chem ozone profiles were completed by climatological ozone profiles between 20 and 40 km, because the convolution by the averaging kernel requires a complete vertical profile, whereas the model is limited to 20 km in altitude.

3.1.1 0–20 km column

Four statistical parameters (described extensively by Kim et al., 2013) are used to analyze the agreement between the observations and model results for the 0–20 km column: the correlation coefficient (R), the normalized mean bias (NMB) and error (NME), and the root mean square error (RMSE). This altitude range includes the lower stratosphere and ozone columns are thus influenced by the large ozone concentrations in this region. The good agreement between models and IASI 0–20 km columns is shown by the results presented in Table 3: the high correlation coefficients ($R > 0.93$, except for WRF-Chem, 0.80) and the low NME (< 20 %) suggest that the models are able to reproduce the ozone columns in summer over Asia.

3.1.2 0–6 km column

Given that the IASI sensor is not particularly sensitive to near-surface trace gas concentrations (Boynard et al., 2009), we focus here on the layer between the ground and 6 km, which is also relevant for regional air quality impacts. This tropospheric layer can also be considered to be less influenced by the stratosphere. Figure 2 shows August 2008 average IASI 0–6 km ozone columns and the smoothed columns using Eq. (1). Statistical parameters (R, NMB, RMSE, NME) based on Fig. 2 are given in Table 4.

ACPD
15, 11049–11109, 2015

The IASI 0–6 km columns in Fig. 2 highlight large ozone concentrations over the eastern coast of China, covering the NCP and YRD regions north of 30° N (5–6 × 10^{17} molec cm^{-2}). At lower latitudes, and particularly over the PRD region, ozone concentrations are lower (3–4 × 10^{17} molec cm^{-2}). The two northerly regions are known for their high emissions of ozone precursors but over the PRD region, as seen in Fig. 1 and discussed in the Introduction, the monsoon flux partially cleans the atmosphere, as well as transporting pollution northward. High concentrations are also observed over Korea, the Sea of Japan, and in the north-eastern part of the evaluation domain which can be attributed to transport of ozone and its precursors from China and Japan (Naja and Akimoto, 2004).

Although the clear separation between high and low concentrations along 30° N and along the Chinese coast is not reproduced by the different models, a significant gradient is nevertheless visible. Moderate ozone concentrations are also observed over the sea of Japan and the north-east part of the domain but this pattern is not reproduced by the models, possibly due to underestimated emissions. Correlation coefficients between the observations and model results reflect the partial restitution of the different patterns by the models. In general, global models tend to overestimate the lower tropospheric ozone columns south of 30° N, and underestimate them slightly to the north (NME around 20 %). Tanimoto et al. (2005) observed a latitudinal gradient in summer due to the Asian monsoon flux. The results presented here suggest that the ECLIPSE models only partially simulate the monsoon flux.

The area delimited in black in Fig. 2 which encompasses regions with high ozone concentrations, namely eastern China, Korea and the Sea of Japan was examined in more detail. Statistical parameters comparing the IASI and smoothed model columns over this region are given in Table 4. The results show that, in general the ECLIPSE models are able to simulate the observed patterns over these regions reasonably well (mean NME of 24 %).

The 0–6 km column provides more precise information than the 0–20 km column about horizontal pollution features. Biases between observations and model results

ACPD
15, 11049–11109, 2015

are similar for 0–20 and 0–6 km ozone columns, suggesting that the models are able to simulate adequately the vertical distribution of tropospheric ozone.

3.2 Tropospheric NO_2 columns

NO_2 is a short-lived species produced largely as a result of rapid interconversion of NO emitted from anthropogenic activities and which can be spectroscopically observed. NO_2 photolysis is the primary source of tropospheric ozone. Investigating how models represent NO_2 can help to understand discrepancies between simulated and observed ozone.

Here, tropospheric NO_2 columns observed by GOME-2 are compared with the model results. Monthly mean observed tropospheric NO_2 columns for August and September 2008, averaged on a regular $1^\circ \times 1^\circ$ grid, are shown in Fig. 3, as well as the absolute differences between the simulated and the observed tropospheric NO_2 columns. Absolute differences are shown instead of the tropospheric columns to highlight the significant bias in the remote region. Since NO_2 has lifetime of only about 1–2 days in the lower troposphere, highest concentrations are observed close to emission areas, i.e., around Beijing and the main cities (Shanghai, Hong-Kong, Seoul, Tokyo). Whilst the models reproduce the patterns over the emission regions, HadGEM, WRF-Chem and NorESM overestimate, and OsloCTM2 and TM4-ECPL underestimate the columns with NMBs of 53, 45, 29, −3 and −11 % and NMEs of 65, 64, 51, 40 and 38 %, respectively.

The same biases are seen over the delimited emission area. In general, biases vary between the models which may point to differences in model chemistry or boundary layer exchange/regional transport, rather than emissions, influencing simulated NO_2 lifetimes.

ACPD
15, 11049–11109, 2015

3.3 Trace gas surface concentrations

Due to the low sensitivity of the IASI sensor close to the surface, it is also necessary to evaluate the models at the surface where air quality issues are important. Surface mixing ratios of ozone and its precursors, as well as SO_2 (an important anthropogenic aerosol precursor), daily model results are compared with ground-based observations at eight sites (SNU and PKU station locations shown in Fig. 1 and coordinates given in Table 2) during August and September 2008. The three first stations (Beijing, Incheon, and Seoul) are urban stations whereas the last five (Gosan, Kunsan, Kangwha, Mokpo, and Taean) are located at rural locations.

Figure 4 shows box and whisker plots for modeled and observed NO_2 mixing ratios. HadGEM and TM4-ECPL are able to reproduce the magnitude of NO_2 surface concentrations at both urban and rural sites. EMEP and WRF-Chem results show better correspondence with measured rural concentrations, whereas they tend to overestimate NO_2 in urban areas, although at the Beijing site, emissions could have been influenced by the mitigation strategies put in place during this period. OsloCTM2 has difficulties reproducing concentrations at both types of site and NorESM underestimates surface NO_2 surface concentrations in general. Given that the models have been run with the same emissions, these differences are likely to be due to differences in loss of NO_2 by OH to form nitric acid in high NO_x environments and subsequent dry or wet deposition. These results are in broad agreement with the tropospheric NO_2 columns shown in Fig. 3.

Modeled CO is also compared to data from eight stations as shown in Fig. 4. In general, observed CO is underestimated by the models at rural stations. Such underestimation over East Asia has already been noted in a multi-model evaluation study by Shindell et al. (2006) and, more globally, in the Northern Hemisphere by Stein et al. (2014). In addition, CO is generally underestimated downwind from source regions, as shown by Shindell et al. (2008) and more recently by Monks et al. (2014). Similarly to the other models (NorESM, OsloCTM2, and TM4-ECPL), the regional model WRF-

ACPD
15, 11049–11109, 2015

Chem shows good agreement with observed CO at urban sites but underestimates CO at rural stations. This may also point to shortcomings in model chemical schemes leading to model CO lifetimes which are too short.

Comparisons with surface ozone data are also presented in Fig. 4. Not surprisingly, higher ozone mixing ratios are observed at the rural stations due to photochemical production downwind from source regions. Differences between the urban and rural stations are reproduced by EMEP, HadGEM and WRF-Chem, whereas TM4-ECPL, OsloCTM2 and NorESM simulate rather constant and too high values of ozone at both urban and rural sites. Global model overestimation of surface ozone is likely to be linked to the underestimation of CO and NO_2.

SO_2 mixing ratios are discussed in Sect. 4.2 together with sulphate.

3.4 Trace gas vertical distributions

Modeled vertical distributions for NO_2, CO, ozone, and SO_2 (hourly or 3 hourly profiles, depending on the model averaged over the measurement period) are compared with observations from the CAREBEIJING 2008 airborne campaign in Fig. 5. The observations are the averages of 12 flights performed between 28 August and 25 September binned by altitude between 500 and 2500 m, providing a good insight into boundary layer (BL) and lower free troposphere pollutant distributions. Three flight routes covering the area 38–40° N and 114–118° E from Tianjin to Shijiazhuang were flown repeatedly. Observations were collected primarily over rural regions but nevertheless show high concentrations of pollutants representative of the large NCP region. Since the dominant winds in summer 2008 were blowing from the South, we estimate the influence of emission mitigation measures applied in the Beijing province on the observations to be limited. Ozone precursors are also elevated up to about 1.5 km showing that the entire boundary layer is influenced by pollution. In general concentrations are lower than observed at the urban surface sites as discussed earlier. Maximum ozone concentrations of more than 100 ppbv were observed in some air masses. Using this

ACPD
15, 11049–11109, 2015

dataset, Zhang et al. (2014) showed that, not surprisingly, the main polluted air masses originate from the urban areas south of the sampling locations.

Observed NO_2 is underestimated by the models at all vertical levels (except HadGEM). This result is consistent with the satellite comparison in Fig. 3 where tropospheric NO_2 columns over the southern Beijing area (where the CAREBEIJING flights were performed) are underestimated by all the models (except HadGEM).

Three models (OsloCTM2, TM4-ECPL, and WRF-Chem) also underestimate the CO mixing ratios, especially between 500 and 1000 m where observed CO reached 0.4 ppbv. This underestimation is consistent with the surface comparisons at rural stations presented in Fig. 4 and with the IASI CO tropospheric columns (not shown).

Comparison with airborne ozone vertical profiles shows that EMEP, TM4-ECPL, and WRF-Chem are able to capture the high concentrations observed below about 750 m albeit with a slight overestimation. All the other models underestimate ozone below this altitude (a result that is somewhat different from the comparison with surface data where models tended to overestimate ozone at rural locations). OsloCTM2 performs better above 750 m whilst other models overestimate concentrations possibly due to too vigorous exchange in the boundary layer as well as too much photochemical ozone production. Solazzo et al. (2013) also identified a similar overestimation in the boundary layer in summer (as part of a regional model evaluation) and suggested this could be due to surface processes. In general, the model performances are consistent with the results presented in the previous section (0–6 km ozone columns).

SO_2 vertical distributions are discussed in Sect. 4.2.

3.5 Discussion

EMEP, as well as WRF-Chem, have a tendency to overestimate NO_2 at polluted urban locations, and given that these two models were run at rather high resolution, may point to an overestimation in the ECLIPSE NO_x emissions. However, comparison against the aircraft profiles, collected in the Beijing region, shows the models are consistently too low making it difficult to conclude on this point. A more consistent pattern is found when

ACPD
15, 11049–11109, 2015

comparing to CO data, with a general underestimation of observed concentrations at the surface and in the lower troposphere. This is more marked at rural locations suggesting potential problems either with transport of polluted air masses from the boundary layer into the free troposphere or that the modeled lifetime of CO (against photochemical OH loss) is too short rather than necessarily an underestimation in emissions. A recent study by Monks et al. (2014) points to these factors to explain the underestimation of CO at mid-latitudes and downwind in the Arctic whereas Stein et al. (2014) noted that the introduction of a seasonal cycle in CO emissions and improvements in the CO dry deposition scheme reduces model biases. There is a tendency for models to overestimate ozone downwind of emission regions at rural sites and compared to aircraft data. This may be due to the general overestimation of background NO_x as shown by comparisons with satellite data. On the other hand, underestimation of NO_2 at polluted sites, appears to result in significant overestimation of ozone in some models (OsloCTM2, TM4-ECPL) likely leading to too little ozone titration in polluted regions. Whilst it is difficult for global models to capture pollutant distributions and gradients between urban and rural environments, these results point to the need to run models at higher resolution in order to correctly simulate the change between ozone titration and production regimes over large polluted conurbations. Evaluation against aircraft data also suggests that models have difficulties simulating high ozone concentrations (more than 100 ppbv) over the Beijing region in summer. This has implications for air quality considerations as well as the amount of ozone (and precursors) transported downwind.

4 Evaluation of modeled aerosol distributions

In this section, model results are evaluated against satellite observations from MODIS and CALIOP instruments, measuring AOD and attenuated backscatter, respectively. MODIS AOD allows a comparison of the total aerosol load integrated over the atmospheric column whereas CALIOP signals are used to evaluate vertical aerosol distributions. Simulated BC, sulphate, and OC are also compared to observations at Beijing

ACPD
15, 11049–11109, 2015

and Gosan ground-based stations as well as with vertical profiles from aerosol LIDAR observations at 10 stations in the Japanese NIES network (white open triangles in Fig. 1).

4.1 Aerosol optical properties

4.1.1 Aerosol optical depth

AOD is determined as the aerosol extinction coefficient integrated over the whole atmospheric column. Since the aerosol extinction coefficient is mostly linked to the aerosol surface distribution (and to a lesser extent to the aerosol complex refractive index), large values of AOD can be observed in cases of high concentrations of fine mode aerosol particles, e.g., pollution over cities (S. Wang et al., 2011). MODIS AOD fields at 550 nm were retrieved from daily observations averaged over August and September 2008, and taking into account missing observations primarily due to the presence of clouds within the column. Days with missing observations were removed from the model results at specific locations. The model results are bi-dimensionally interpolated on the 1° × 1° MODIS grid.

Figure 6 (top panels) shows average maps of observed and simulated AODs at 550 nm. In general, the models correctly represent the main features of the spatial AOD distribution, including the large values over the NCP area and over northern India. However, AODs are not reproduced equally accurately by the models, especially over these two regions. Absolute differences between the models and MODIS are also shown in Fig. 6 (bottom panels). HadGEM and, to a lesser extent, NorESM overestimate AOD background values. In addition, HadGEM and EMEP overestimate AODs over NCP whereas they are underestimated by ECHAM6-HAM2, OsloCTM2, and WRF-Chem.

Several reasons might explain such discrepancies. Different treatments of aerosol emissions within the models can influence the AOD, especially, assumptions about the size distribution of particle emissions. All aerosols, including dust and sea salt particles can affect observed AOD, and biases in the simulated aerosol concentrations and sizes

ACPD
15, 11049–11109, 2015

impact AOD estimates. Aerosol removal processes (i.e., dry and wet deposition) also play an important role in the aerosol loading and resulting AODs.

In order to further investigate model skill at simulating AOD, two specific regions with high AOD values are selected within the domain and are shown in the top left panel of Fig. 6. The first region is located over northern India and is well known for the significant accumulation of pollutants at this time of the year, driven by the Indian monsoon. This accumulation is due to large local emissions, and the effect of dominant southerly winds causing the transport of pollution up to the Himalayas which acts as a natural barrier (Lawrence and Lelieveld, 2010). The second region encompasses the main emission areas in eastern China, including several megacities such as Beijing, Shanghai, and Hong-Kong. Whilst this region is influenced by dust episodes coming from the north-eastern Asian deserts (e.g., Huang et al., 2013) in spring, the monsoon flux inhibits such events in summer.

Figure 7 compares MODIS and model mean/percentile AODs over these regions and the rest of the domain during August and September 2008. In terms of AOD variability, the agreement is generally better over eastern China than over northern India. More specifically, over eastern China, NorESM and TM4-ECPL capture the observed variability with a deviation of less than 10 % whereas it is somewhat overestimated by HadGEM and EMEP and underestimated by ECHAM6-HAM2 and WRF-Chem. Over northern India, observed variability is reproduced by the HadGEM, OsloCTM2 and WRF-Chem models with deviations from the MODIS observations of less than 25 %, whereas it is underestimated by the other models. The corresponding statistical parameters are summarized in Table 6 for the two regions and in Table 7 for the entire domain.

ACPD
15, 11049–11109, 2015

4.1.2 Aerosol backscatter coefficient

Evaluation against satellite observations

In this section, the ECLIPSE models are evaluated against vertical distributions of attenuated backscatter at 532 nm from CALIOP, averaged over a $3^\circ \times 5^\circ$ grid over Asia for August and September 2008. As indicated in Table 1, most of the models calculated the aerosol extinction coefficient (α) rather than the aerosol backscatter (β). Though CALIPSO level 3 data from the operational algorithm includes α, important uncertainties are associated with these retrievals. This is because α retrievals rely on inversion of lidar signals, which requires knowledge of the so-called Lidar ratio $S = \frac{\alpha_{aer}}{\beta_{aer}}$, dependent on the aerosol type. Omar et al. (2010) showed that a low SNR (Signal to Noise Ratio) can lead to mis-classification and lack of aerosol layer identification, especially close to the surface. Liu et al. (2009) noted cloud contamination in backscatter and α profiles, whereas Young and Vaughan (2009) pointed out potentially erroneous assumptions in the lidar ratio S used in α retrievals. Finally, Winker et al. (2009) highlighted calibration coefficient biases in the daytime attenuated backscatter profiles.

To verify the possible aerosol mis-classification, an alternative product based on the CALIOP level 1 data and presented by Ancellet et al. (2014) is used. This product is based on level 1 backscatter signals filtered for clouds using CALIPSO level 2 cloud masks. In this retrieval, 3 brightness temperatures (8, 10, 12 µm), measured by the infrared interferometer on CALIPSO, the cloud layer depolarization ratio and the color ratio are used as additional requirements. The final product described in Ancellet et al. (2014) is unitless and is called the apparent (or attenuated) scattering ratio (R_{app}). This product is not affected by errors associated with the lidar signal inversion. To allow a fair comparison, model results must be converted to R_{app} using:

$$R_{app}(z) = \frac{\beta(z)}{\beta_{mol}(z)} \times \exp\left(-2\int_{z}^{z_{ref}} \alpha_{aer}(z')\mathrm{d}z'\right). \quad (2)$$

ACPD
15, 11049–11109, 2015

β and α can be described as the sum of molecular (β_{mol} and α_{mol}) and aerosol (β_{aer} and α_{aer}) signals which describe the backscatter and extinction associated with trace gases and aerosols, respectively. z_{ref} is an altitude where only the molecular signal is observed. For some models, α only is provided. In this case, R_{app} is calculated using:

$$R_{app}(z) = \frac{\alpha_{aer,\,model}(z) \times BER + \beta_{mol}(z)}{\beta_{mol}(z)} \times \exp\left(-2\int_{z}^{z_{ref}} \alpha_{mol}(z')dz'\right), \quad (3)$$

where BER is the backscatter to extinction ratio ($BER = \frac{\beta_{aer}}{\alpha_{aer}}$) and is fixed to $0.02\,sr^{-1}$ which is a common value observed over east-Asia (Cattrall et al., 2005; Xie et al., 2008; Chiang et al., 2008). BER is the only assumption made in the R_{app} calculation.

The distribution pattern of CALIPSO-derived R_{app} between 0 and 2 km (Fig. 8a) highlights three major features over Asia, consistent with the MODIS observations presented in Fig. 6. They are associated with polluted regions over eastern China and northern India where anthropogenic emissions are significant, and background pollution over the desert region, north-west of the Himalayas. The ECLIPSE models reproduce the location of anthropogenic plumes over eastern China but underestimate the magnitude by 5–50 %. One exception is EMEP which overestimates the backscatter signal by more than 50 %. Only OsloCTM2 and EMEP simulate the observed pattern over northern India, albeit with a slight overestimation (20–40 %). The signal over the Tibetan plateau desert which is mostly due to dust particles is not simulated by the models.

Between 2 and 4 km (Fig. 8b), CALIOP detected elevated aerosols over the Tibetan plateau and eastern China. Again, none of the models are able to reproduce the signal over the desert region. However, the models (except NorESM) are able to capture a higher R_{app} over eastern China. Whereas most models overestimate the observed signals, it is slightly under predicted by WRF-Chem (10 %). Two models (WRF-Chem and ECHAM6-HAM2) simulate aerosols at this altitude range over northern India, which probably corresponding to those detected by CALIOP between 0 and 2 km.

ACPD
15, 11049–11109, 2015

Above 4 km (not shown), CALIOP only observes a significant signal over the Tibetan plateau region North of the Himalayas, whereas WRF-Chem and ECHAM6-HAM2 simulate backscatter signal over the northern India and all the models, with the exception of NorESM, simulate some aerosols in the middle troposphere over eastern China.

This suggests that these models are overestimating transport of pollution into the free troposphere or that loss by wet scavenging is insufficient. This finding is in agreement with previous work noting overestimation of observed aerosol concentrations in the free troposphere (Koffi et al., 2012; Samset et al., 2014). We also note that, compared to CALIPSO, some of the models (NorESM, and to a lesser extent EMEP and OsloCTM2), simulate high amounts of aerosols below 2 km in the northeast of the domain (south of the Kamtchatka peninsula). This is due to elevated sulphate in these models (not shown).

Evaluation against ground-based observations

Good model skill in simulating aerosol vertical distributions is essential for reliable aerosol radiative forcing estimations (Boucher et al., 2013). Whilst evaluation against CALIOP is made with the data averaged over large grid boxes due to the scarcity of satellite overpasses, simulated optical properties are also compared with aerosol lidar measurements collected at sites in the Japanese NIES network. In order to allow a fair comparison, the simulated extinction and observed backscatter are converted to R_{app}, as described in Sect. 4.1.2. All the NIES stations are at urban locations and the R_{app} profiles calculated from observations reveal large aerosol loads in the boundary layer and up to 3 km at certain stations.

The R_{app} mean profiles at each station are shown in Fig. 9. In general, ECHAM6-HAM2 and NorESM underestimate the R_{app} between the surface and 2 km whereas average profiles (shape and intensity) from EMEP, OsloCTM2 and WRF-Chem are in a fair agreement with the observations. Over 2 km, the models adequately simulate R_{app} values. These results are not always in agreement with the model comparison against MODIS and CALIOP observations. For example, the EMEP model overes-

ACPD
15, 11049–11109, 2015

timates the spaceborne derived backscatter signal over Japan (see Fig. 8a and b) whereas it is in agreement with the ground-based lidar observations. ECHAM6-HAM2 and NorESM also show ambiguous results since the backscatter signal observed by CALIOP is overestimated by both models whereas they underestimate the signals provided by the ground-based lidars. These discrepancies may be due to (i) CALIOP uncertainties at lower altitudes, especially over complex topography, and (ii) low model resolution making it difficult for models to capture lidar profiles obtained in urban areas (NIES). On the other hand, CALIOP signals are averaged over urban, rural and marine regions.

The mean altitude Z_{mean} of the NIES lidar profiles, which provides information on the profile shape, is calculated for each profile by a weighting function following:

$$Z_{\text{mean}} = \frac{\sum_{\text{level}=1}^{n} (R_{\text{app},i} - 1)^2 \times Z_i}{\sum_{i=1}^{n} (R_{\text{app},i} - 1)^2}. \quad (4)$$

Modeled overestimation of this quantity implies an underestimation of low altitude signals and/or an overestimation of signals at higher altitudes. In general, Z_{mean} is overestimated by the models. EMEP and ECHAM6-HAM2 simulate Z_{mean} with an error of less than 300 m, OsloCTM2 and WRF-Chem errors are around 1 km, and finally the NorESM mean error is 2 km. Such biases are likely to be due to coarse model resolutions that are unable to adequately describe variations between rural, maritime, and peri-urban areas, leading to an underestimation of the high backscatter value usually observed in the boundary layer in the urban area where the NIES lidar are operating.

4.2 Aerosol composition

In this section, modeled aerosol components which are important for estimation of anthropogenic radiative forcing (BC, OC, and sulphate) are compared with the ground-

ACPD
15, 11049–11109, 2015

based observations at Beijing and Gosan as shown in Fig. 10. As noted earlier, pollutant concentrations in Beijing are mainly influenced by local emissions, whereas pollution at Gosan is transported from the Asian continent (Kim et al., 2007). In addition, as noted earlier, anthropogenic emissions in the Beijing area were reduced during summer 2008, with probable impacts on observed pollutant amounts (Y. Wang et al., 2009; Wang et al., 2010). BC originates from primary emissions due to incomplete combustion, whereas OC and sulphate are emitted from primary sources or formed as secondary products following oxidation of precursors. BC concentrations are mainly influenced by emissions and deposition. On the other hand, OC and sulphate aerosols are more hydrophilic and may react with gaseous species. Their mass therefore evolves as a function of gas condensation at their surface, in addition to primary emissions, oxidation and deposition.

Mean observed concentrations of BC, OC and sulphate during August and September 2008 are 2.0, 15.4, and 12.1 $\mu g\,m^{-3}$ at the Beijing site compared to 0.18, 1.3 and 7.4 $\mu g\,m^{-3}$, respectively at Gosan, the latter being consistent with observations from this site reported by Sun et al. (2004). In general, the models capture the observed BC mass concentrations at Gosan but most models overpredict BC over Beijing, possibly a result of emission measures in place from mid-August to mid-September 2008. OsloCTM2 simulates well the gradient in concentrations between polluted and downwind locations whereas NorESM, which simulates polluted concentrations reasonably well, has too little BC downwind at Gosan.

ECHAM6-HAM2, TM4-ECPL, and WRF-Chem capture observed OC concentrations fairly well in Beijing but they are underestimated at Gosan. NorESM and OsloCTM2 have very low (factor ×3) OC over polluted Beijing and downwind over Gosan whereas EMEP largely overestimates OC in Gosan. These discrepancies, whilst based on comparisons with rather limited data, support global model evaluations (e.g., Tsigaridis et al., 2014) showing that models have problems simulating OC and has implications with regard to estimates of radiative forcing from these aerosols.

ACPD
15, 11049–11109, 2015

This also applies to radiative forcing estimates due to sulphate aerosols which, as shown in Fig. 10, is the most abundant aerosol component measured at the sites considered here. At the polluted Beijing site, observed sulphate concentrations are largely over-predicted by ECHAM6-HAM2, EMEP, and TM4-ECPL. This is linked to the overestimation of SO_2 as shown in Fig. 4. ECHAM6-HAM2 also overestimates sulphate at Gosan, whereas they are lower than observed in the EMEP results, suggesting that sulphate may be lost too fast in this model. This also appears to be the case for NorESM which has very low sulphate at Gosan. HadGEM, OsloCTM2, and WRF-Chem capture the concentrations reasonably well at both two sites. These findings are similar to those found when evaluating modeled optical properties (AOD and R_{app}) over eastern China.

5 Summary and discussion

The ability of six global chemical-aerosol/chemistry-climate models and one regional chemical aerosol model to simulate distributions of short-lived climate pollutants is evaluated over Asia during summer 2008 using satellite and in-situ observations. The models were run with the same ECLIPSE anthropogenic emissions and the same biomass burning dataset. Where possible models were also nudged with relevant meteorological analyses.

Ozone precursors (NO_2 and CO) are in general underestimated by the models in the troposphere, with the notable exception of surface NO_2 concentrations possibly suggesting that these emission are too high. The CO underestimation, mostly seen in rural areas, is most likely due to too short lifetimes (against photochemical OH loss) in models as well as underestimation of transport from the boundary layer to the free troposphere. Ozone columns and vertical profiles are generally well captured. In contrast, global models have difficulties simulating ozone gradients at the surface between urban and rural environments. These findings point to the need to employ adequate model resolution in order to improve simulated responses to emissions when moving from ozone titration to ozone production regimes within large polluted conurbations,

ACPD
15, 11049–11109, 2015

their surroundings and downwind. This has implications for the use of global models to assess regional air quality as well as climate impacts of tropospheric ozone.

Model results are compared to aerosol optical depths, as well as aerosol scattering ratios observed by MODIS and CALIOP, respectively, showing enhanced aerosol concentrations over eastern China and northern India. Over both regions, AOD predictions are model-dependent: only certain models are able to adequately reproduce summertime average MODIS AODs over eastern China (NorESM, TM4-ECPL and WRF-Chem), and over northern India (HadGEM, OsloCTM2 and WRF-Chem). In general, similar results are found when comparing to CALIOP aerosol scattering ratios. Aerosol vertical distributions between 0 and 4 km over the desert regions are not really captured at all, whereas the spatial distributions over eastern China and northern India are reasonably well simulated by most models. However, important model biases are seen in the signal intensity, suggesting that models are unable to simulate the correct amount of aerosol species with high scattering efficiency like sulphate and to a lesser extent OC. Evaluation against ground-based aerosol lidar profiles at urban locations over Japan show inconsistencies with the CALIOP comparison which can be attributed to differences in spatial representativeness of the different measurement types.

Overall, the ECLIPSE model evaluation highlights significant differences between the models and observations, even when models are run using the same emissions. Better general agreement is found for trace gases compared to aerosols, for which model simulations are very variable. For both trace gases and aerosols, models have difficulties reproducing gradients between urban and rural (downwind) locations. Improved model resolution as well as improved understanding and model treatments of processes affecting pollutant lifetimes are needed. Model evaluations using a variety of observation types are required so that difference aspects of model behavior can be tested. Results from this study suggest that significant uncertainties still exist in chemistry-climate simulations which has implications for the use of such models in the assessment of radiative effects of short-lived climate forcers on climate and regional/global air quality.

ACPD
15, 11049–11109, 2015

Acknowledgements. The authors would like to thank the European Union for funding the FP7 ECLIPSE project (grant agreement no. 282688). Jerome Fast (PNNL) is acknowledged for providing advice about the WRF-Chem simulations. This work was granted access to the HPC resources of IDRIS under the allocation 2014-017141 made by GENCI (Grand Equipement National de Calcul Intensif). Computing resources were also provided by the IPSL CICLAD/CLIMSERV mesocenter. The MODIS data used in this study were acquired as part of the NASA's Earth-Sun System Division and archived/distributed by the MODIS Adaptive Processing System (MODAPS). We also acknowledge the free use of tropospheric NO_2 column data from the GOME-2 sensor from www.temis.nl. IASI is a joint mission of EUMETSAT and the Centre National d'Etudes Spatiales (CNES, France). We are grateful to Juliette Hadji-Lazaro (LATMOS), Pierre Coheur and Daniel Hurtmans (ULB) for providing the IASI O3-FORLI data. S.-W. Kim was supported by the KMA R&D (CATER 2012–3020) and by the Korean Ministry of Environment as "Climate Change Correspondence".

References

Ackerman, A. S., Toon, O. B., Stevens, D. E., Heymsfield, A. J., Ramanathan, V., and Welton, E. J.: Reduction of tropical cloudiness by soot, Science, 288, 1042–1047, doi:10.1126/science.288.5468.1042, 2000. 11053

Albrecht, B. A.: Aerosols, cloud microphysics, and fractional cloudiness, Science, 245, 1227–1230, doi:10.1126/science.245.4923.1227, 1989. 11053

Allen, R. J. and Landuyt, W.: The vertical distribution of black carbon in CMIP5 models: comparison to observations and the importance of convective transport, J. Geophys. Res.-Atmos., 119, 4808–4835, doi:10.1002/2014JD021595, 2014. 11054

Ancellet, G., Pelon, J., Blanchard, Y., Quennehen, B., Bazureau, A., Law, K. S., and Schwarzenboeck, A.: Transport of aerosol to the Arctic: analysis of CALIOP and French aircraft data during the spring 2008 POLARCAT campaign, Atmos. Chem. Phys., 14, 8235–8254, doi:10.5194/acp-14-8235-2014, 2014. 11070

Anenberg, S., Schwartz, J., Shindell, D., Amann, M., Faluvegi, G., Klimont, Z., Janssens-Maenhout, G., Pozzoli, L., Van Dingenen, R., Vignati, E., Emberson, L., Muller, N. Z., West, J. J., Williams, M., Demkine, V., Hicks, W. K., Kuylenstierna, J., Raes, F., and Ramanathan, V.: Global air quality and health co-benefits of mitigating near-term climate change

ACPD
15, 11049–11109, 2015

through methane and black carbon emission controls, 120, Environ. Health Persp., 831–839, doi:10.1289/ehp.1104301, 2012. 11051

Bentsen, M., Bethke, I., Debernard, J. B., Iversen, T., Kirkevåg, A., Seland, Ø., Drange, H., Roelandt, C., Seierstad, I. A., Hoose, C., and Kristjánsson, J. E.: The Norwegian Earth System Model, NorESM1-M – Part 1: Description and basic evaluation of the physical climate, Geosci. Model Dev., 6, 687–720, doi:10.5194/gmd-6-687-2013, 2013. 11093

Boersma, K. F., Eskes, H. J., and Brinksma, E. J.: Error analysis for tropospheric NO_2 retrieval from space, J. Geophys. Res.-Atmos., 109, D04311, doi:10.1029/2003JD003962, 2004. 11058

Bond, T. C., Doherty, S. J., Fahey, D. W., Forster, P. M., Berntsen, T., DeAngelo, B. J., Flanner, M. G., Ghan, S., Kärcher, B., Koch, D., Kinne, S., Kondo, Y., Quinn, P. K., Sarofim, M. C., Schultz, M. G., Schulz, M., Venkataraman, C., Zhang, H., Zhang, S., Bellouin, N., Guttikunda, S. K., Hopke, P. K., Jacobson, M. Z., Kaiser, J. W., Klimont, Z., Lohmann, U., Schwarz, J. P., Shindell, D., Storelvmo, T., Warren, S. G., and Zender, C. S.: Bounding the role of black carbon in the climate system: a scientific assessment, J. Geophys. Res.-Atmos., 118, 5380–5552, doi:10.1002/jgrd.50171, 2013. 11053, 11054

Boucher, O., Randall, D., Artaxo, P., Bretherton, C., Feingold, G., Forster, P., Kerminen, V.-M., Kondo, Y., Liao, H., Lohmann, U., Rasch, P., Satheesh, S. K., Sherwood, S., Stevens, B., and Zhang, X. Y.: Clouds and aerosols, in: Climate Change 2013: the Physical Science Basis. Contribution of Working Group I to the Fifth Assessment Report of the Intergovernmental Panel on Climate Change, edited by: Stocker, T. F., Qin, D., Plattner, G.-K., Tignor, M., Allen, S. K., Boschung, J., Nauels, A., Xia, Y., Bex, V., and Midgley, P. M., Cambridge University Press, Cambridge, UK, New York, NY, USA, 2013. 11072

Boynard, A., Clerbaux, C., Coheur, P.-F., Hurtmans, D., Turquety, S., George, M., Hadji-Lazaro, J., Keim, C., and Meyer-Arnek, J.: Measurements of total and tropospheric ozone from IASI: comparison with correlative satellite, ground-based and ozonesonde observations, Atmos. Chem. Phys., 9, 6255–6271, doi:10.5194/acp-9-6255-2009, 2009. 11061

Boynard, A., Clerbaux, C., Clarisse, L., Safieddine, S., Pommier, M., Van Damme, M., Bauduin, S., Oudot, C., Hadji-Lazaro, J., Hurtmans, D., and Coheur, P.-F.: First simultaneous space measurements of atmosph eric pollutants in the boundary layer from IASI: a case study in the North China Plain, Geophys. Res. Lett., 41, 645–651, doi:10.1002/2013GL058333, 2014. 11052

ACPD
15, 11049–11109, 2015

Buhaug, O., Corbett, J., Endresen, O., Eyring, V., Faber, J., Hanayama, S., Lee, D. S., Lee, D., Lindstad, H., Markowska, A., Mjelde, A., Nelissen, D., Nilsen, J., Palsson, C., Winebrake, J., Wu, W., and Yoshida, K.: Second IMO GHG study 2009, Tech. rep., International Maritime Organization (IMO), London, UK, 2009. 11057

Cao, J., Lee, S., Ho, K., Zou, S., Fung, K., Li, Y., Watson, J. G., and Chow, J. C.: Spatial and seasonal variations of atmospheric organic carbon and elemental carbon in pearl river delta region, china, Atmos. Environ., 38, 4447–4456, doi:10.1016/j.atmosenv.2004.05.016, 2004. 11054

Cattrall, C., Reagan, J., Thome, K., and Dubovik, O.: Variability of aerosol and spectral lidar and backscatter and extinction ratios of key aerosol types derived from selected Aerosol Robotic Network locations, J. Geophys. Res.-Atmos., 110, D10S11, doi:10.1029/2004JD005124, 2005. 11071

Chan, C. K. and Yao, X.: Air pollution in mega cities in china, Atmos. Environ., 42, 1–42, doi:10.1016/j.atmosenv.2007.09.003, 2008. 11052

Chen, J., Zhao, C. S., Ma, N., Liu, P. F., Göbel, T., Hallbauer, E., Deng, Z. Z., Ran, L., Xu, W. Y., Liang, Z., Liu, H. J., Yan, P., Zhou, X. J., and Wiedensohler, A.: A parameterization of low visibilities for hazy days in the North China Plain, Atmos. Chem. Phys., 12, 4935–4950, doi:10.5194/acp-12-4935-2012, 2012. 11054

Cherian, R., Quaas, J., Salzmann, M., and Wild, M.: Pollution trends over Europe constrain global aerosol forcing as simulated by climate models, Geophys. Res. Lett., 41, 2176–2181, doi:10.1002/2013GL058715, 2014. 11053

Chiang, C.-W., Das, S. K., and Nee, J.-B.: An iterative calculation to derive extinction-to-backscatter ratio based on lidar measurements, J. Quant. Spectrosc. Ra., 109, 1187–1195, doi:10.1016/j.jqsrt.2007.10.011, 2008. 11071

Chou, C. C.-K., Tsai, C.-Y., Chang, C.-C., Lin, P.-H., Liu, S. C., and Zhu, T.: Photochemical production of ozone in Beijing during the 2008 Olympic Games, Atmos. Chem. Phys., 11, 9825–9837, doi:10.5194/acp-11-9825-2011, 2011. 11058

Clerbaux, C., Boynard, A., Clarisse, L., George, M., Hadji-Lazaro, J., Herbin, H., Hurtmans, D., Pommier, M., Razavi, A., Turquety, S., Wespes, C., and Coheur, P.-F.: Monitoring of atmospheric composition using the thermal infrared IASI/MetOp sounder, Atmos. Chem. Phys., 9, 6041–6054, doi:10.5194/acp-9-6041-2009, 2009. 11057

ACPD
15, 11049–11109, 2015

Daskalakis, N., Myriokefalitakis, S., and Kanakidou, M.: Sensitivity of tropospheric loads and lifetimes of short lived pollutants to fire emissions, Atmos. Chem. Phys., 15, 3543–3563, doi:10.5194/acp-15-3543-2015, 2015. 11093

Ding, A. J., Wang, T., Thouret, V., Cammas, J.-P., and Nédélec, P.: Tropospheric ozone climatology over Beijing: analysis of aircraft data from the MOZAIC program, Atmos. Chem. Phys., 8, 1–13, doi:10.5194/acp-8-1-2008, 2008. 11052

Dufour, G., Eremenko, M., Orphal, J., and Flaud, J.-M.: IASI observations of seasonal and day-to-day variations of tropospheric ozone over three highly populated areas of China: Beijing, Shanghai, and Hong Kong, Atmos. Chem. Phys., 10, 3787–3801, doi:10.5194/acp-10-3787-2010, 2010. 11052

Flowers, B. A., Dubey, M. K., Mazzoleni, C., Stone, E. A., Schauer, J. J., Kim, S.-W., and Yoon, S. C.: Optical-chemical-microphysical relationships and closure studies for mixed carbonaceous aerosols observed at Jeju Island; 3-laser photoacoustic spectrometer, particle sizing, and filter analysis, Atmos. Chem. Phys., 10, 10387–10398, doi:10.5194/acp-10-10387-2010, 2010. 11056, 11058

Fuelberg, H. E., Kiley, C. M., Hannan, J. R., Westberg, D. J., Avery, M. A., and Newell, R. E.: Meteorological conditions and transport pathways during the transport and chemical evolution over the Pacific (TRACE-P) experiment, J. Geophys. Res.-Atmos., 108, 8782, doi:10.1029/2002JD003092, 2003. 11053

Gao, L., Zhang, M., and Han, Z.: Model analysis of seasonal variations in tropospheric ozone and carbon monoxide over East Asia, Adv. Atmos. Sci., 26, 312–318, doi:10.1007/s00376-009-0312-9, 2009. 11053

Grell, G. A., Peckham, S. E., Schmitz, R., McKeen, S. A., Frost, G., Skamarock, W. C., and Eder, B.: Fully coupled "online" chemistry within the WRF model, Atmos. Environ., 39, 6957–6975, doi:10.1016/j.atmosenv.2005.04.027, 2005. 11093

Guenther, A., Hewitt, C. N., Erickson, D., Fall, R., Geron, C., Graedel, T., Harley, P., Klinger, L., Lerdau, M., Mckay, W. A., Pierce, T., Scholes, B., Steinbrecher, R., Tallamraju, R., Taylor, J., and Zimmerman, P.: A global model of natural volatile organic compound emissions, J. Geophys. Res.-Atmos., 100, 8873–8892, doi:10.1029/94JD02950, 1995. 11093

Guenther, A., Karl, T., Harley, P., Wiedinmyer, C., Palmer, P. I., and Geron, C.: Estimates of global terrestrial isoprene emissions using MEGAN (Model of Emissions of Gases and Aerosols from Nature), Atmos. Chem. Phys., 6, 3181–3210, doi:10.5194/acp-6-3181-2006, 2006. 11093

ACPD
15, 11049–11109, 2015

Han, Z., Sakurai, T., Ueda, H., Carmichael, G., Streets, D., Hayami, H., Wang, Z., Holloway, T., Engardt, M., Hozumi, Y., Park, S., Kajino, M., Sartelet, K., Fung, C., Bennet, C., Thongboonchoo, N., Tang, Y., Chang, A., Matsuda, K., and Amann, M.: Mics-asia II: model intercomparison and evaluation of ozone and relevant species, Atmos. Environ., 42, 3491–3509, doi:10.1016/j.atmosenv.2007.07.031,2008. 11053

Haywood, J. M. and Shine, K. P.: The effect of anthropogenic sulfate and soot aerosol on the clear sky planetary radiation budget, Geophys. Res. Lett., 22, 603–606, doi:10.1029/95GL00075, 1995. 11053

He, Y. J., Uno, I., Wang, Z. F., Pochanart, P., Li, J., and Akimoto, H.: Significant impact of the East Asia monsoon on ozone seasonal behavior in the boundary layer of Eastern China and the west Pacific region, Atmos. Chem. Phys., 8, 7543–7555, doi:10.5194/acp-8-7543-2008, 2008. 11052, 11053, 11059

Hewitt, H. T., Copsey, D., Culverwell, I. D., Harris, C. M., Hill, R. S. R., Keen, A. B., McLaren, A. J., and Hunke, E. C.: Design and implementation of the infrastructure of HadGEM3: the next-generation Met Office climate modelling system, Geosci. Model Dev., 4, 223–253, doi:10.5194/gmd-4-223-2011, 2011. 11093

Huang, X.-F., He, L.-Y., Hu, M., and Zhang, Y.-H.: Annual variation of particulate organic compounds in $PM_{2.5}$ in the urban atmosphere of beijing, Atmos. Environ., 40, 2449–2458, doi:10.1016/j.atmosenv.2005.12.039, 2006. 11054

Huang, X.-F., He, L.-Y., Hu, M., Canagaratna, M. R., Sun, Y., Zhang, Q., Zhu, T., Xue, L., Zeng, L.-W., Liu, X.-G., Zhang, Y.-H., Jayne, J. T., Ng, N. L., and Worsnop, D. R.: Highly time-resolved chemical characterization of atmospheric submicron particles during 2008 Beijing Olympic Games using an Aerodyne High-Resolution Aerosol Mass Spectrometer, Atmos. Chem. Phys., 10, 8933–8945, doi:10.5194/acp-10-8933-2010, 2010. 11055, 11058

Huang, X.-X., Wang, T.-J., Jiang, F., Liao, J.-B., Cai, Y.-F., Yin, C.-Q., Zhu, J.-L., and Han, Y.: Studies on a severe dust storm in East Asia and its impact on the air quality of Nanjing, China, Aerosol Air Qual. Res., 13, 179–193, doi:10.4209/aaqr.2012.05.0108, 2013. 11057, 11069

Hubanks, P. A., King, M. D., Latnick, S. P., and Pincus, R.: MODIS Algorithm Theoretical Basis Document No. ATBD-MOD-30 for Level-3 Global Gridded Atmosphere Products (08_D3, 08_E3, 08_M3), available at: http://modis-atmos.gsfc.nasa.gov/MOD08_M3/atbd.html (last access: 14 April 2015), 2008. 11058

ACPD
15, 11049–11109, 2015

Hurtmans, D., Coheur, P.-F., Wespes, L., Clarisse, L., Scharf, O., Clerbaux, C., Hadji-Lazaro, J., George, M., and Turquety, S.: FORLI radiative transfer and retrieval code for IASI, J. Quant. Spectrosc. Ra., 113, 1391–1408, 2012. 11057

Iversen, T., Bentsen, M., Bethke, I., Debernard, J. B., Kirkevåg, A., Seland, Ø., Drange, H., Kristjansson, J. E., Medhaug, I., Sand, M., and Seierstad, I. A.: The Norwegian Earth System Model, NorESM1-M – Part 2: Climate response and scenario projections, Geosci. Model Dev., 6, 389–415, doi:10.5194/gmd-6-389-2013, 2013. 11093

Jackson, S. C.: Parallel pursuit of near-term and long-term climate mitigation, Science, 326, 526–527, doi:10.1126/science.1177042, 2009. 11051

Jaffe, D., Anderson, T., Covert, D., Kotchenruther, R., Trost, B., Danielson, J., Simpson, W., Berntsen, T., Karlsdottir, S., Blake, D., Harris, J., Carmichael, G., and Uno, I.: Transport of Asian air pollution to North America, Geophys. Res. Lett., 26, 711–714, doi:10.1029/1999GL900100, 1999. 11055

Kanakidou, M., Duce, R. A., Prospero, J. M., Baker, A. R., Benitez-Nelson, C., Dentener, F. J., Hunter, K. A., Liss, P. S., Mahowald, N., Okin, G. S., Sarin, M., Tsigaridis, K., Uematsu, M., Zamora, L. M., and Zhu, T.: Atmospheric fluxes of organic N and P to the global ocean, Global Biogeochem. Cy., 26, GB3026, doi:10.1029/2011GB004277, 2012. 11093

Kim, S.-W., Yoon, S.-C., Jefferson, A., Ogren, J. A., Dutton, E. G., Won, J.-G., Ghim, Y. S., Lee, B.-I., and Han, J.-S.: Aerosol optical, chemical and physical properties at gosan, korea during asian dust and pollution episodes in 2001, Atmos. Environ., 39, 39–50, doi:10.1016/j.atmosenv.2004.09.056, 2005. 11058

Kim, S.-W., Yoon, S.-C., Kim, J., and Kim, S.-Y.: Seasonal and monthly variations of columnar aerosol optical properties over east Asia determined from multi-year MODIS, LIDAR, and {AERONET} sun/sky radiometer measurements, Atmos. Environ., 41, 1634–1651, doi:10.1016/j.atmosenv.2006.10.044, 2007. 11054, 11056, 11057, 11074

Kim, Y., Sartelet, K., Raut, J.-C., and Chazette, P.: Evaluation of the weather research and forecast/urban model over Greater Paris, Bound.-Lay. Meteorol., 149, 105–132, doi:10.1007/s10546-013-9838-6, 2013. 11061

Kinne, S., Schulz, M., Textor, C., Guibert, S., Balkanski, Y., Bauer, S. E., Berntsen, T., Berglen, T. F., Boucher, O., Chin, M., Collins, W., Dentener, F., Diehl, T., Easter, R., Feichter, J., Fillmore, D., Ghan, S., Ginoux, P., Gong, S., Grini, A., Hendricks, J., Herzog, M., Horowitz, L., Isaksen, I., Iversen, T., Kirkevåg, A., Kloster, S., Koch, D., Kristjansson, J. E., Krol, M., Lauer, A., Lamarque, J. F., Lesins, G., Liu, X., Lohmann, U., Montanaro, V.,

ACPD
15, 11049–11109, 2015

Myhre, G., Penner, J., Pitari, G., Reddy, S., Seland, O., Stier, P., Takemura, T., and Tie, X.: An AeroCom initial assessment – optical properties in aerosol component modules of global models, Atmos. Chem. Phys., 6, 1815–1834, doi:10.5194/acp-6-1815-2006, 2006. 11054

Kirkevåg, A., Iversen, T., Seland, Ø., Hoose, C., Kristjánsson, J. E., Struthers, H., Ekman, A. M. L., Ghan, S., Griesfeller, J., Nilsson, E. D., and Schulz, M.: Aerosol–climate interactions in the Norwegian Earth System Model – NorESM1-M, Geosci. Model Dev., 6, 207–244, doi:10.5194/gmd-6-207-2013, 2013. 11093

Klimont, Z., Smith, S. J., and Cofala, J.: The last decade of global anthropogenic sulfur dioxide: 2000–2011 emissions, Environ. Res. Lett., 8, 014003, doi:10.1088/1748-9326/8/1/014003, 2013. 11052

Klimont, Z., et al.: ECLIPSE emissions, in preparation, 2015. 11052, 11056

Koch, D., Schulz, M., Kinne, S., McNaughton, C., Spackman, J. R., Balkanski, Y., Bauer, S., Berntsen, T., Bond, T. C., Boucher, O., Chin, M., Clarke, A., De Luca, N., Dentener, F., Diehl, T., Dubovik, O., Easter, R., Fahey, D. W., Feichter, J., Fillmore, D., Freitag, S., Ghan, S., Ginoux, P., Gong, S., Horowitz, L., Iversen, T., Kirkevåg, A., Klimont, Z., Kondo, Y., Krol, M., Liu, X., Miller, R., Montanaro, V., Moteki, N., Myhre, G., Penner, J. E., Perlwitz, J., Pitari, G., Reddy, S., Sahu, L., Sakamoto, H., Schuster, G., Schwarz, J. P., Seland, Ø., Stier, P., Takegawa, N., Takemura, T., Textor, C., van Aardenne, J. A., and Zhao, Y.: Evaluation of black carbon estimations in global aerosol models, Atmos. Chem. Phys., 9, 9001–9026, doi:10.5194/acp-9-9001-2009, 2009. 11054

Koffi, B., Schulz, M., Bréon, F.-M., Griesfeller, J., Winker, D., Balkanski, Y., Bauer, S., Berntsen, T., Chin, M., Collins, W. D., Dentener, F., Diehl, T., Easter, R., Ghan, S., Ginoux, P., Gong, S., Horowitz, L. W., Iversen, T., Kirkevåg, A., Koch, D., Krol, M., Myhre, G., Stier, P., and Takemura, T.: Application of the CALIOP layer product to evaluate the vertical distribution of aerosols estimated by global models: AeroCom phase I results, J. Geophys. Res.-Atmos., 117, D10201, doi:10.1029/2011JD016858, 2012. 11054, 11072

Lawrence, M. G. and Lelieveld, J.: Atmospheric pollutant outflow from southern Asia: a review, Atmos. Chem. Phys., 10, 11017–11096, doi:10.5194/acp-10-11017-2010, 2010. 11069

Lee, D. S., Fahey, D. W., Forster, P. M., Newton, P. J., Wit, R. C., Lim, L. L., Owen, B., and Sausen, R.: Aviation and global climate change in the 21st century, Atmos. Environ., 43, 3520–3537, doi:10.1016/j.atmosenv.2009.04.024, 2009. 11057

ACPD
15, 11049–11109, 2015

Li, J., Wang, Z., Akimoto, H., Gao, C., Pochanart, P., and Wang, X.: Modeling study of ozone seasonal cycle in lower troposphere over east Asia, J. Geophys. Res.-Atmos., 112, D22S25, doi:10.1029/2006JD008209, 2007. 11053

Li, J., Wang, Z., Huang, H., Hu, M., Meng, F., Sun, Y., Wang, X., Wang, Y., and Wang, Q.: Assessing the effects of trans-boundary aerosol transport between various city clusters on regional haze episodes in spring over East China, Tellus B, 65, 20052, doi:10.3402/tellusb.v65i0.20052, 2013. 11054

Lin, M., Holloway, T., Oki, T., Streets, D. G., and Richter, A.: Multi-scale model analysis of boundary layer ozone over East Asia, Atmos. Chem. Phys., 9, 3277–3301, doi:10.5194/acp-9-3277-2009, 2009. 11052, 11053

Lin, W., Xu, X., Zhang, X., and Tang, J.: Contributions of pollutants from North China Plain to surface ozone at the Shangdianzi GAW Station, Atmos. Chem. Phys., 8, 5889–5898, doi:10.5194/acp-8-5889-2008, 2008. 11052

Liu, H., Jacob, D. J., Chan, L. Y., Oltmans, S. J., Bey, I., Yantosca, R. M., Harris, J. M., Duncan, B. N., and Martin, R. V.: Sources of tropospheric ozone along the Asian Pacific Rim: an analysis of ozonesonde observations, J. Geophys. Res.-Atmos., 107, ACH3.1–ACH3.19, doi:10.1029/2001JD002005, 2002. 11052

Liu, Z., Vaughan, M., Winker, D., Kittaka, C., Getzewich, B., Kuehn, R., Omar, A., Powell, K., Trepte, C., and Hostetler, C.: The CALIPSO lidar cloud and aerosol discrimination: version 2 algorithm and initial assessment of performance, J. Atmos. Ocean. Tech., 26, 1198–1213, doi:10.1175/2009JTECHA1229.1, 2009. 11070

Ma, J., Chen, Y., Wang, W., Yan, P., Liu, H., Yang, S., Hu, Z., and Lelieveld, J.: Strong air pollution causes widespread haze-clouds over China, J. Geophys. Res.-Atmos., 115, D18204, doi:10.1029/2009JD013065, 2010. 11052

Ma, J., Xu, X., Zhao, C., and Yan, P.: A review of atmospheric chemistry research in China: photochemical smog, haze pollution, and gas-aerosol interactions, Adv. Atmos. Sci., 29, 1006–1026, doi:10.1007/s00376-012-1188-7, 2012. 11052

Mann, G. W., Carslaw, K. S., Spracklen, D. V., Ridley, D. A., Manktelow, P. T., Chipperfield, M. P., Pickering, S. J., and Johnson, C. E.: Description and evaluation of GLOMAP-mode: a modal global aerosol microphysics model for the UKCA composition-climate model, Geosci. Model Dev., 3, 519–551, doi:10.5194/gmd-3-519-2010, 2010. 11093

McCormick, R. A. and Ludwig, J. H.: Climate modification by atmospheric aerosols, Science, 156, 1358–1359, doi:10.1126/science.156.3780.1358, 1967. 11053

ACPD
15, 11049–11109, 2015

Monks, S. A., Arnold, S. R., Emmons, L. K., Law, K. S., Turquety, S., Duncan, B. N., Flemming, J., Huijnen, V., Tilmes, S., Langner, J., Mao, J., Long, Y., Thomas, J. L., Steenrod, S. D., Raut, J. C., Wilson, C., Chipperfield, M. P., Diskin, G. S., Weinheimer, A., Schlager, H., and Ancellet, G.: Multi-model study of chemical and physical controls on transport of anthropogenic and biomass burning pollution to the Arctic, Atmos. Chem. Phys., 15, 3575–3603, doi:10.5194/acp-15-3575-2015, 2015. 11064, 11067

Munro, R., Perez Albiñana, A., Callies, J., Corpaccioli, E., Eisinger, M., Lefebvre, A., and Hahne, A.: Expectations for GOME-2 on the METOP satellites, in: ERS-Envisat Symposium "Looking Down to Earth in the New Millennium", European Space Agency (Special Publication) ESA SP, Gothenburg, 221–227, 2000. 11058

Myhre, G., Berglen, T. F., Johnsrud, M., Hoyle, C. R., Berntsen, T. K., Christopher, S. A., Fahey, D. W., Isaksen, I. S. A., Jones, T. A., Kahn, R. A., Loeb, N., Quinn, P., Remer, L., Schwarz, J. P., and Yttri, K. E.: Modelled radiative forcing of the direct aerosol effect with multi-observation evaluation, Atmos. Chem. Phys., 9, 1365–1392, doi:10.5194/acp-9-1365-2009, 2009. 11093

Myhre, G., Shindell, D., Bréon, F.-M., Collins, W., Fuglestvedt, J., Huang, J., Koch, D., Lamarque, J.-F., Lee, D., Mendoza, B., Nakajima, T., Robock, A., Stephens, G., Takemura, T., and Zhang, H.: Anthropogenic and natural radiative forcing, in: Climate Change 2013: the Physical Science Basis. Contribution of Working Group I to the Fifth Assessment Report of the Intergovernmental Panel on Climate Change, edited by: Stocker, T. F., Qin, D., Plattner, G.-K., Tignor, M., Allen, S. K., Boschung, J., Nauels, A., Xia, Y., Bex, V., and Midgley, P. M., Cambridge University Press, Cambridge, UK, New York, NY, USA, 2013. 11052, 11053, 11054

Myriokefalitakis, S., Tsigaridis, K., Mihalopoulos, N., Sciare, J., Nenes, A., Kawamura, K., Segers, A., and Kanakidou, M.: In-cloud oxalate formation in the global troposphere: a 3-D modeling study, Atmos. Chem. Phys., 11, 5761–5782, doi:10.5194/acp-11-5761-2011, 2011. 11093

Naja, M. and Akimoto, H.: Contribution of regional pollution and long-range transport to the Asia-Pacific region: analysis of long-term ozonesonde data over Japan, J. Geophys. Res.-Atmos., 109, D21306, doi:10.1029/2004JD004687, 2004. 11053, 11062

Nawahda, A., Yamashita, K., Ohara, T., Kurokawa, J., and Yamaji, K.: Evaluation of premature mortality caused by exposure to $PM_{2.5}$ and ozone in East Asia: 2000, 2005, 2020, Water Air Soil Poll., 223, 3445–3459, doi:10.1007/s11270-012-1123-7,2012. 11054

ACPD
15, 11049–11109, 2015

Omar, A., Liu, Z., Vaughan, M., Thornhill, K., Kittaka, C., Ismail, S., Hu, Y., Chen, G., Powell, K., Winker, D., Trepte, C., Winstead, E., and Anderson, B.: Extinction-to-backscatter ratios of Saharan dust layers derived from in situ measurements and CALIPSO overflights during NAMMA, J. Geophys. Res.-Atmos., 115, D24217, doi:10.1029/2010JD014223, 2010. 11070

Penner, J. E., Prather, M. J., Isaksen, I. S. A., Fuglestvedt, J. S., Klimont, Z., and Stevenson, D. S.: Short-lived uncertainty?, Nat. Geosci., 3, 587–588, doi:10.1038/ngeo932, 2010. 11051

Pruppacher, H. R. and Klett, J. D.: Microphysics of Clouds and Precipitation, D. Reidel Publishing Company, 2nd Edn., Kluwer Academic Publishers, Dordrecht, The Netherlands, 1978. 11051

Ramanathan, V. and Carmichael, G.: Global and regional climate changes due to black carbon, Nat. Geosci., 1, 221–227, doi:10.1038/ngeo156, 2008. 11051

Richter, A., Burrows, J. P., Nusz, H., Granier, C., and Niemeier, U.: Increase in tropospheric nitrogen dioxide over China observed from space, Nature, 437, 129–132, doi:10.1038/nature04092, 2005. 11052

Rogelj, J., Schaeffer, M., Meinshausen, M., Shindell, D. T., Hare, W., Klimont, Z., Velders, G. J. M., Amann, M., and Schellnhuber, H. J.: Disentangling the effects of CO_2 and short-lived climate forcer mitigation, P. Natl. Acad. Sci. USA, 111, 16325–16330, doi:10.1073/pnas.1415631111, 2014. 11051

Roiger, A., Schlager, H., Schäfler, A., Huntrieser, H., Scheibe, M., Aufmhoff, H., Cooper, O. R., Sodemann, H., Stohl, A., Burkhart, J., Lazzara, M., Schiller, C., Law, K. S., and Arnold, F.: In-situ observation of Asian pollution transported into the Arctic lowermost stratosphere, Atmos. Chem. Phys., 11, 10975–10994, doi:10.5194/acp-11-10975-2011, 2011. 11055

Safieddine, S., Clerbaux, C., George, M., Hadji-Lazaro, J., Hurtmans, D., Coheur, P.-F., Wespes, C., Loyola, D., Valks, P., and Hao, N.: Tropospheric ozone and nitrogen dioxide measurements in urban and rural regions as seen by IASI and GOME-2, J. Geophys. Res.-Atmos., 118, 10555–10566, doi:10.1002/jgrd.50669, 2013. 11052, 11053

Saide, P. E., Spak, S. N., Carmichael, G. R., Mena-Carrasco, M. A., Yang, Q., Howell, S., Leon, D. C., Snider, J. R., Bandy, A. R., Collett, J. L., Benedict, K. B., de Szoeke, S. P., Hawkins, L. N., Allen, G., Crawford, I., Crosier, J., and Springston, S. R.: Evaluating WRF-Chem aerosol indirect effects in Southeast Pacific marine stratocumulus during VOCALS-REx, Atmos. Chem. Phys., 12, 3045–3064, doi:10.5194/acp-12-3045-2012, 2012. 11057

ACPD
15, 11049–11109, 2015

Samset, B. H., Myhre, G., Schulz, M., Balkanski, Y., Bauer, S., Berntsen, T. K., Bian, H., Bellouin, N., Diehl, T., Easter, R. C., Ghan, S. J., Iversen, T., Kinne, S., Kirkevåg, A., Lamarque, J.-F., Lin, G., Liu, X., Penner, J. E., Seland, Ø., Skeie, R. B., Stier, P., Takemura, T., Tsigaridis, K., and Zhang, K.: Black carbon vertical profiles strongly affect its radiative forcing uncertainty, Atmos. Chem. Phys., 13, 2423–2434, doi:10.5194/acp-13-2423-2013, 2013. 11054

Samset, B. H., Myhre, G., Herber, A., Kondo, Y., Li, S.-M., Moteki, N., Koike, M., Oshima, N., Schwarz, J. P., Balkanski, Y., Bauer, S. E., Bellouin, N., Berntsen, T. K., Bian, H., Chin, M., Diehl, T., Easter, R. C., Ghan, S. J., Iversen, T., Kirkevåg, A., Lamarque, J.-F., Lin, G., Liu, X., Penner, J. E., Schulz, M., Seland, Ø., Skeie, R. B., Stier, P., Takemura, T., Tsigaridis, K., and Zhang, K.: Modelled black carbon radiative forcing and atmospheric lifetime in AeroCom Phase II constrained by aircraft observations, Atmos. Chem. Phys., 14, 12465–12477, doi:10.5194/acp-14-12465-2014, 2014. 11072

Shao, M., Tang, X., Zhang, Y., and Li, W.: City clusters in China: air and surface water pollution, Front. Ecol. Environ., 4, 353–361, doi:10.1890/1540-9295(2006)004[0353:CCICAA]2.0.CO;2, 2006. 11052

Shimizu, A., Sugimoto, N., Matsui, I., Arao, K., Uno, I., Murayama, T., Kagawa, N., Aoki, K., Uchiyama, A., and Yamazaki, A.: Continuous observations of Asian dust and other aerosols by polarization lidars in China and Japan during ACE-Asia, J. Geophys. Res.-Atmos., 109, D19S17, doi:10.1029/2002JD003253, 2004. 11059

Shindell, D., Kuylenstierna, J. C. I., Vignati, E., van Dingenen, R., Amann, M., Klimont, Z., Anenberg, S. C., Muller, N., Janssens-Maenhout, G., Raes, F., Schwartz, J., Faluvegi, G., Pozzoli, L., Kupiainen, K., Höglund-Isaksson, L., Emberson, L., Streets, D., Ramanathan, V., Hicks, K., Oanh, N. T. K., Milly, G., Williams, M., Demkine, V., and Fowler, D.: Simultaneously mitigating near-term climate change and improving human health and food security, Science, 335, 183–189, doi:10.1126/science.1210026, 2012. 11051

Shindell, D. T., Faluvegi, G., Stevenson, D. S., Krol, M. C., Emmons, L. K., Lamarque, J.-F., Pétron, G., Dentener, F. J., Ellingsen, K., Schultz, M. G., Wild, O., Amann, M., Atherton, C. S., Bergmann, D. J., Bey, I., Butler, T., Cofala, J., Collins, W. J., Derwent, R. G., Doherty, R. M., Drevet, J., Eskes, H. J., Fiore, A. M., Gauss, M., Hauglustaine, D. A., Horowitz, L. W., Isaksen, I. S. A., Lawrence, M. G., Montanaro, V., Müller, J.-F., Pitari, G., Prather, M. J., Pyle, J. A., Rast, S., Rodriguez, J. M., Sanderson, M. G., Savage, N. H., Strahan, S. E., Sudo, K., Szopa, S., Unger, N., van Noije, T. P. C., and Zeng, G.: Multimodel simulations of carbon

ACPD
15, 11049–11109, 2015

monoxide: comparison with observations and projected near-future changes, J. Geophys. Res.-Atmos., 111, D19306, doi:10.1029/2006JD007100, 2006. 11064

Shindell, D. T., Chin, M., Dentener, F., Doherty, R. M., Faluvegi, G., Fiore, A. M., Hess, P., Koch, D. M., MacKenzie, I. A., Sanderson, M. G., Schultz, M. G., Schulz, M., Stevenson, D. S., Teich, H., Textor, C., Wild, O., Bergmann, D. J., Bey, I., Bian, H., Cuvelier, C., Duncan, B. N., Folberth, G., Horowitz, L. W., Jonson, J., Kaminski, J. W., Marmer, E., Park, R., Pringle, K. J., Schroeder, S., Szopa, S., Takemura, T., Zeng, G., Keating, T. J., and Zuber, A.: A multi-model assessment of pollution transport to the Arctic, Atmos. Chem. Phys., 8, 5353–5372, doi:10.5194/acp-8-5353-2008, 2008. 11064

Shoemaker, J. K., Schrag, D. P., Molina, M. J., and Ramanathan, V.: What role for short-lived climate pollutants in mitigation policy?, Science, 342, 1323–1324, doi:10.1126/science.1240162, 2013. 11051

Simpson, D., Benedictow, A., Berge, H., Bergström, R., Emberson, L. D., Fagerli, H., Flechard, C. R., Hayman, G. D., Gauss, M., Jonson, J. E., Jenkin, M. E., Nyíri, A., Richter, C., Semeena, V. S., Tsyro, S., Tuovinen, J.-P., Valdebenito, Á., and Wind, P.: The EMEP MSC-W chemical transport model – technical description, Atmos. Chem. Phys., 12, 7825–7865, doi:10.5194/acp-12-7825-2012, 2012. 11093

Sindelarova, K., Granier, C., Bouarar, I., Guenther, A., Tilmes, S., Stavrakou, T., Müller, J.-F., Kuhn, U., Stefani, P., and Knorr, W.: Global data set of biogenic VOC emissions calculated by the MEGAN model over the last 30 years, Atmos. Chem. Phys., 14, 9317–9341, doi:10.5194/acp-14-9317-2014, 2014. 11093

Skeie, R. B., Berntsen, T. K., Myhre, G., Tanaka, K., Kvalevåg, M. M., and Hoyle, C. R.: Anthropogenic radiative forcing time series from pre-industrial times until 2010, Atmos. Chem. Phys., 11, 11827–11857, doi:10.5194/acp-11-11827-2011, 2011. 11093

Smith, S. J. and Mizrahi, A.: Near-term climate mitigation by short-lived forcers, P. Natl. Acad. Sci. USA, 110, 14202–14206, doi:10.1073/pnas.1308470110, 2013. 11051

Solazzo, E., Bianconi, R., Pirovano, G., Moran, M. D., Vautard, R., Hogrefe, C., Appel, K. W., Matthias, V., Grossi, P., Bessagnet, B., Brandt, J., Chemel, C., Christensen, J. H., Forkel, R., Francis, X. V., Hansen, A. B., McKeen, S., Nopmongcol, U., Prank, M., Sartelet, K. N., Segers, A., Silver, J. D., Yarwood, G., Werhahn, J., Zhang, J., Rao, S. T., and Galmarini, S.: Evaluating the capability of regional-scale air quality models to capture the vertical distribution of pollutants, Geosci. Model Dev., 6, 791–818, doi:10.5194/gmd-6-791-2013, 2013. 11066

ACPD
15, 11049–11109, 2015

Stein, O., Schultz, M. G., Bouarar, I., Clark, H., Huijnen, V., Gaudel, A., George, M., and Clerbaux, C.: On the wintertime low bias of Northern Hemisphere carbon monoxide found in global model simulations, Atmos. Chem. Phys., 14, 9295–9316, doi:10.5194/acp-14-9295-2014, 2014. 11064, 11067

Stevens, B., Giorgetta, M., Esch, M., Mauritsen, T., Crueger, T., Rast, S., Salzmann, M., Schmidt, H., Bader, J., Block, K., Brokopf, R., Fast, I., Kinne, S., Kornblueh, L., Lohmann, U., Pincus, R., Reichler, T., and Roeckner, E.: Atmospheric component of the MPI-M Earth System Model: ECHAM6, Journal of Advances in Modeling Earth Systems, 5, 146–172, doi:10.1002/jame.20015, 2013. 11093

Stevenson, D. S., Dentener, F. J., Schultz, M. G., Ellingsen, K., van Noije, T. P. C., Wild, O., Zeng, G., Amann, M., Atherton, C. S., Bell, N., Bergmann, D. J., Bey, I., Butler, T., Cofala, J., Collins, W. J., Derwent, R. G., Doherty, R. M., Drevet, J., Eskes, H. J., Fiore, A. M., Gauss, M., Hauglustaine, D. A., Horowitz, L. W., Isaksen, I. S. A., Krol, M. C., Lamarque, J.-F., Lawrence, M. G., Montanaro, V., Müller, J.-F., Pitari, G., Prather, M. J., Pyle, J. A., Rast, S., Rodriguez, J. M., Sanderson, M. G., Savage, N. H., Shindell, D. T., Strahan, S. E., Sudo, K., and Szopa, S.: Multimodel ensemble simulations of present-day and near-future tropospheric ozone, J. Geophys. Res.-Atmos., 111, D08301, doi:10.1029/2005JD006338, 2006. 11052

Streets, D. G., Bond, T. C., Carmichael, G. R., Fernandes, S. D., Fu, Q., He, D., Klimont, Z., Nelson, S. M., Tsai, N. Y., Wang, M. Q., Woo, J.-H., and Yarber, K. F.: An inventory of gaseous and primary aerosol emissions in Asia in the year 2000, J. Geophys. Res.-Atmos., 108, 8809, doi:10.1029/2002JD003093, 2003. 11052, 11056

Sugimoto, N., Matsui, I., Shimizu, A., Nishizawa, T., Hara, Y., Xie, C., Uno, I., Yumimoto, K., Wang, Z., and Yoon, S.-C.: Lidar network observations of tropospheric aerosols, ProcSPIE, 7153, 71530A, doi:10.1117/12.806540, 2008. 11059

Sun, Y., Zhuang, G., Wang, Y., Han, L., Guo, J., Dan, M., Zhang, W., Wang, Z., and Hao, Z.: The air-borne particulate pollution in Beijing: concentration, composition, distribution and sources, Atmos. Environ., 38, 5991–6004, doi:10.1016/j.atmosenv.2004.07.009, 2004. 11054, 11074

Tanimoto, H., Sawa, Y., Matsueda, H., Uno, I., Ohara, T., Yamaji, K., Kurokawa, J.-I., and Yonemura, S.: Significant latitudinal gradient in the surface ozone spring maximum over East Asia, Geophys. Res. Lett., 32, L21805, doi:10.1029/2005GL023514, 2005. 11062

Tsigaridis, K., Daskalakis, N., Kanakidou, M., Adams, P. J., Artaxo, P., Bahadur, R., Balkanski, Y., Bauer, S. E., Bellouin, N., Benedetti, A., Bergman, T., Berntsen, T. K., Beukes, J. P.,

ACPD
15, 11049–11109, 2015

Bian, H., Carslaw, K. S., Chin, M., Curci, G., Diehl, T., Easter, R. C., Ghan, S. J., Gong, S. L., Hodzic, A., Hoyle, C. R., Iversen, T., Jathar, S., Jimenez, J. L., Kaiser, J. W., Kirkevåg, A., Koch, D., Kokkola, H., Lee, Y. H, Lin, G., Liu, X., Luo, G., Ma, X., Mann, G. W., Mihalopoulos, N., Morcrette, J.-J., Müller, J.-F., Myhre, G., Myriokefalitakis, S., Ng, N. L., O'Donnell, D., Penner, J. E., Pozzoli, L., Pringle, K. J., Russell, L. M., Schulz, M., Sciare, J., Seland, Ø., Shindell, D. T., Sillman, S., Skeie, R. B., Spracklen, D., Stavrakou, T., Steenrod, S. D., Takemura, T., Tiitta, P., Tilmes, S., Tost, H., van Noije, T., van Zyl, P. G., von Salzen, K., Yu, F., Wang, Z., Wang, Z., Zaveri, R. A., Zhang, H., Zhang, K., Zhang, Q., and Zhang, X.: The AeroCom evaluation and intercomparison of organic aerosol in global models, Atmos. Chem. Phys., 14, 10845–10895, doi:10.5194/acp-14-10845-2014, 2014. 11074

Twomey, S.: The influence of pollution on the shortwave albedo of clouds, J. Atmos. Sci., 34, 1149–1152, doi:10.1175/1520-0469(1977)034<1149:TIOPOT>2.0.CO;2, 1977. 11053

van der Werf, G. R., Randerson, J. T., Giglio, L., Collatz, G. J., Mu, M., Kasibhatla, P. S., Morton, D. C., DeFries, R. S., Jin, Y., and van Leeuwen, T. T.: Global fire emissions and the contribution of deforestation, savanna, forest, agricultural, and peat fires (1997–2009), Atmos. Chem. Phys., 10, 11707–11735, doi:10.5194/acp-10-11707-2010, 2010. 11057

Wang, B., Shao, M., Lu, S. H., Yuan, B., Zhao, Y., Wang, M., Zhang, S. Q., and Wu, D.: Variation of ambient non-methane hydrocarbons in Beijing city in summer 2008, Atmos. Chem. Phys., 10, 5911–5923, doi:10.5194/acp-10-5911-2010, 2010. 11055, 11074

Wang, R., Tao, S., Shen, H., Huang, Y., Chen, H., Balkanski, Y., Boucher, O., Ciais, P., Shen, G., Li, W., Zhang, Y., Chen, Y., Lin, N., Su, S., Li, B., Liu, J., and Liu, W.: Trend in global black carbon emissions from 1960 to 2007, Environ. Sci. Technol., 48, 6780–6787, doi:10.1021/es5021422, 2014. 11052

Wang, S., Fang, L., Gu, X., Yu, T., and Gao, J.: Comparison of aerosol optical properties from Beijing and Kanpur, Atmos. Environ., 45, 7406–7414, doi:10.1016/j.atmosenv.2011.06.055, 2011. 11068

Wang, T. and Xie, S.: Assessment of traffic-related air pollution in the urban streets before and during the 2008 Beijing Olympic Games traffic control period, Atmos. Environ., 43, 5682–5690, doi:10.1016/j.atmosenv.2009.07.034, 2009. 11055

Wang, T., Wei, X. L., Ding, A. J., Poon, C. N., Lam, K. S., Li, Y. S., Chan, L. Y., and Anson, M.: Increasing surface ozone concentrations in the background atmosphere of Southern China, 1994–2007, Atmos. Chem. Phys., 9, 6217–6227, doi:10.5194/acp-9-6217-2009, 2009. 11052

ACPD
15, 11049–11109, 2015

Wang, Y., Hao, J., McElroy, M. B., Munger, J. W., Ma, H., Chen, D., and Nielsen, C. P.: Ozone air quality during the 2008 Beijing Olympics: effectiveness of emission restrictions, Atmos. Chem. Phys., 9, 5237–5251, doi:10.5194/acp-9-5237-2009, 2009. 11055, 11074

Wang, Y., Zhang, Y., Hao, J., and Luo, M.: Seasonal and spatial variability of surface ozone over China: contributions from background and domestic pollution, Atmos. Chem. Phys., 11, 3511–3525, doi:10.5194/acp-11-3511-2011, 2011. 11052

Winker, D. M., Hunt, W. H., and McGill, M. J.: Initial performance assessment of CALIOP, Geophys. Res. Lett., 34, L19803, doi:10.1029/2007GL030135, 2007. 11058

Winker, D. M., Vaughan, M. A., Omar, A., Hu, Y., Powell, K. A., Liu, Z., Hunt, W. H., and Young, S. A.: Overview of the CALIPSO mission and CALIOP data processing algorithms, J. Atmos. Ocean. Tech., 26, 2310–2323, doi:10.1175/2009JTECHA1281.1, 2009. 11070

Worden, H. M., Cheng, Y., Pfister, G., Carmichael, G. R., Zhang, Q., Streets, D. G., Deeter, M., Edwards, D. P., Gille, J. C., and Worden, J. R.: Satellite-based estimates of reduced CO and CO_2 emissions due to traffic restrictions during the 2008 Beijing Olympics, Geophys. Res. Lett., 39, L14802, doi:10.1029/2012GL052395, 2012. 11055

Xie, C., Nishizawa, T., Sugimoto, N., Matsui, I., and Wang, Z.: Characteristics of aerosol optical properties in pollution and Asian dust episodes over Beijing, China, Appl. Optics, 47, 4945–4951, doi:10.1364/AO.47.004945, 2008. 11071

Xu, X., Lin, W., Wang, T., Yan, P., Tang, J., Meng, Z., and Wang, Y.: Long-term trend of surface ozone at a regional background station in eastern China 1991–2006: enhanced variability, Atmos. Chem. Phys., 8, 2595–2607, doi:10.5194/acp-8-2595-2008, 2008. 11052

Yang, F., He, K., Ye, B., Chen, X., Cha, L., Cadle, S. H., Chan, T., and Mulawa, P. A.: One-year record of organic and elemental carbon in fine particles in downtown Beijing and Shanghai, Atmos. Chem. Phys., 5, 1449–1457, doi:10.5194/acp-5-1449-2005, 2005. 11054

Yang, F., Tan, J., Zhao, Q., Du, Z., He, K., Ma, Y., Duan, F., Chen, G., and Zhao, Q.: Characteristics of $PM_{2.5}$ speciation in representative megacities and across China, Atmos. Chem. Phys., 11, 5207–5219, doi:10.5194/acp-11-5207-2011, 2011. 11052

Young, S. A. and Vaughan, M. A.: The retrieval of profiles of particulate extinction from Cloud-Aerosol Lidar Infrared Pathfinder Satellite Observations (CALIPSO) data: algorithm description, J. Atmos. Ocean. Tech., 26, 1105–1119, doi:10.1175/2008JTECHA1221.1, 2009. 11070

Zhang, K., O'Donnell, D., Kazil, J., Stier, P., Kinne, S., Lohmann, U., Ferrachat, S., Croft, B., Quaas, J., Wan, H., Rast, S., and Feichter, J.: The global aerosol-climate model ECHAM-

ACPD
15, 11049–11109, 2015

HAM, version 2: sensitivity to improvements in process representations, Atmos. Chem. Phys., 12, 8911–8949, doi:10.5194/acp-12-8911-2012, 2012. 11093

Zhang, M., Uno, I., Zhang, R., Han, Z., Wang, Z., and Pu, Y.: Evaluation of the Models-3 Community Multi-scale Air Quality (CMAQ) modeling system with observations obtained during the trace-p experiment: comparison of ozone and its related species, Atmos. Environ., 40, 4874–4882, doi:10.1016/j.atmosenv.2005.06.063, 2006. 11053

Zhang, W., Zhu, T., Yang, W., Bai, Z., Sun, Y. L., Xu, Y., Yin, B., and Zhao, X.: Airborne measurements of gas and particle pollutants during CAREBeijing-2008, Atmos. Chem. Phys., 14, 301–316, doi:10.5194/acp-14-301-2014, 2014. 11055, 11059, 11066

Zhao, P., Zhang, X., Xu, X., and Zhao, X.: Long-term visibility trends and characteristics in the region of Beijing, Tianjin, and Hebei, China, Atmos. Res., 101, 711–718, doi:10.1016/j.atmosres.2011.04.019,2011. 11054

Zhou, Y., Wu, Y., Yang, L., Fu, L., He, K., Wang, S., Hao, J., Chen, J., and Li, C.: The impact of transportation control measures on emission reductions during the 2008 Olympic Games in Beijing, China, Atmos. Environ., 44, 285–293, doi:10.1016/j.atmosenv.2009.10.040, 2010. 11055

ACPD
15, 11049–11109, 2015

Table 1. ECLIPSE model description including meteorological fields used to nudge simulations (where applicable), spatial resolution, aerosol schemes, and biogenic emissions. Trace gases, aerosol species and optical parameters output by the models are provided together with references for the different models. Institutes responsible for each model are indicated with the indices of the author affiliations.

Models	Met. fields	Horizontal Res.	Vertical levels	Aerosol parameterisation	Biogenic emissions
ECHAM6-HAM2[10]	Nudged to ECMWF	1.8° × 1.8°	31	7 aerosol modes (HAM2)	Guenther 1990 (Guenther et al., 1995)
EMEP[4]	ECMWF	1° × 1°	20	fine and coarse mode	Guenther 1990 (Guenther et al., 1995)
HadGEM3[5,11]	Nudged to ECMWF	1.25° × 1.875°	63	GLOMAP-mode scheme	Guenther 1995 (Guenther et al., 1995)
NorESM[3,4]	online	1.9° × 2.5°	26	mass/species (13 modes)	MEGAN v2 (Guenther et al., 2006)
OsloCTM2[3]	ECMWF-IFS	2.81° × 2.81°	60	bulk aerosol scheme	Guenther 1990 (Guenther et al., 1995)
TM4-ECPL[6,7]	ECMWF-ERA INTERIM	2° × 3°	34	fine and coarse modes	MEGAN-MACC (Sindelarova et al., 2014)
WRF-Chem[1]	NCEP FNL	50 km × 50 km	49	8 bins/species 40–10 000 nm	MEGAN v2 (Guenther et al., 2006)

Models	Trace gases	Aerosol comp.	Optical param.	References
ECHAM6-HAM2	SO_2	BC, OC, SO_4	AOD, α_{550}	Stevens et al. (2013), Zhang et al. (2012)
EMEP	CO, O_3, NO_2, SO_2	BC, OC, SO_4	AOD, α_{550}	Simpson et al. (2012)
HadGEM3	CO, O_3, NO_2, SO_2	BC, SO_4	AOD	Mann et al. (2010), Hewitt et al. (2011)
NorESM	CO, O_3, NO_2, SO_2	BC, OC, SO_4	AOD, β_{550}	Kirkevåg et al. (2013), Iversen et al. (2013), Bentsen et al. (2013)
OsloCTM2	CO, O_3, NO_2	BC, OC, SO_4	AOD, α_{550}	Myhre et al. (2009), Skeie et al. (2011)
TM4-ECPL	CO, O_3, NO_2, SO_2	BC, OC, SO_4	AOD	Myriokefalitakis et al. (2011), Kanakidou et al. (2012), Daskalakis et al. (2015)
WRF-Chem	CO, O_3, NO_2, SO_2	BC, OC, SO_4	AOD, β_{550}	Grell et al. (2005)

ACPD
15, 11049–11109, 2015

Table 2. Coordinates of stations used in this study and available parameters.

Station	Country	longitude (° E)	latitude (° N)	Available parameters
Beijing	China	116.3	40.0	CO, NO_2, O_3, SO_2, BC, OC, SO_4
Gosan	South Korea	126.2	33.3	CO, NO_2, O_3, SO_2, BC, OC, SO_4
Inchon		126.6	37.5	CO, NO_2, O_3, SO_2
Kangwha		126.3	37.7	CO, NO_2, O_3, SO_2
Kunsan		126.7	36.0	CO, NO_2, O_3, SO_2
Mokpo		126.4	34.8	CO, NO_2, O_3, SO_2
Seoul		127.0	37.6	CO, NO_2, O_3, SO_2
Taean		126.4	39.7	CO, NO_2, O_3, SO_2
Chiba	Japan	140.1	36.0	β_{532}
Fukue		128.7	32.7	β_{532}
Matsue		133.0	35.5	β_{532}
Nagasaki		130.0	32.9	β_{532}
Niigata		138.9	37.8	β_{532}
Osaka		135.6	34.6	β_{532}
Sapporo		141.3	43.1	β_{532}
Tokyo		139.7	35.7	β_{532}
Toyama		137.1	36.7	β_{532}
Tsukuba		140.1	36.0	β_{532}

ACPD
15, 11049–11109, 2015

Table 3. Statistical parameters (correlation coefficient R, normalized mean bias NMB, root mean square error RMSE, and normalized mean error NME) for model simulations of 0–20 km ozone column over Asia in August 2008 compared to the IASI ozone-FORLI observations.

Models	R	NMB (%)	RMSE (molec cm^{-2})	NME (%)
HadGEM	0.95	9.4	2.50×10^{17}	10.4
NorESM	0.93	10.1	2.86×10^{17}	11.8
OsloCTM2	0.96	−0.01	1.48×10^{17}	5.4
TM4-ECPL	0.98	9.6	2.90×10^{17}	10.7
WRF-Chem	0.80	−17.5	5.36×10^{17}	18.1
Model mean	0.97	25.0	1.30×10^{17}	5.2

ACPD
15, 11049–11109, 2015

Table 4. Statistical parameters (correlation coefficient R, normalized mean bias NMB, root mean square error RMSE, and normalized mean error NME) calculated using simulations of the 0–6 km ozone columns over Asia (left parameters) and over the high concentration columns delimited in black in Fig. 2 (right parameters) in August 2008 by the ECLIPSE models compared to the IASI ozone-FORLI observations.

	Asia				High ozone region			
Models	R	NMB (%)	RMSE (molec cm^{-2})	NME (%)	R	NMB (%)	RMSE (molec cm^{-2})	NME (%)
HadGEM	0.76	15.4	0.93×10^{17}	18.5	0.72	12.1	1.09×10^{17}	24.3
NorESM	0.82	16.7	0.88×10^{17}	19.0	0.62	7.0	1.28×10^{17}	28.3
OsloCTM2	0.56	3.0	1.03×10^{17}	23.0	0.51	−3.9	1.40×10^{17}	32.9
TM4-ECPL	0.63	8.9	0.93×10^{17}	19.8	0.65	7.5	1.16×10^{17}	24.7
WRF-Chem	0.69	30.2	1.45×10^{17}	31.8	0.66	23.6	1.46×10^{17}	35.2
Model mean	0.76	13.5	0.87×10^{17}	18.1	0.72	12.2	1.10×10^{17}	24.1

ACPD
15, 11049–11109, 2015

Table 5. Statistical parameters (correlation coefficient R, normalized mean bias NMB, root mean square error RMSE, and normalized mean error NME) for model simulations of NO_2 tropospheric columns over Asia and over Chinese emission area shown in Fig. 3 averaged over August and September 2008 compared to GOME-2 satellite observations.

	Asia				Chinese emissions area			
Models	R	NMB (%)	RMSE (molec cm^{-2})	NME (%)	R	NMB (%)	RMSE (molec cm^{-2})	NME (%)
HadGEM	0.76	53.1	1.91×10^{15}	65.4	0.78	30.1	2.90×10^{15}	59.5
NorESM	0.80	29.1	1.27×10^{15}	50.7	0.75	8.1	2.63×10^{15}	47.9
OsloCTM2	0.76	−3.1	1.19×10^{15}	40.1	0.68	−19.8	2.80×10^{15}	51.4
TM4-ECPL	0.81	−11.6	1.09×10^{15}	38.5	0.81	−18.1	2.23×10^{15}	38.7
WRF-Chem	0.77	45.3	1.31×10^{15}	64.5	0.79	13.2	2.33×10^{15}	53.9
Model mean	0.84	22.6	1.04×10^{15}	41.1	0.83	−4.1	2.14×10^{15}	37.8

ACPD
15, 11049–11109, 2015

Table 6. Deviation (in %) of model results from MODIS AODs observations: mean, median, differences between 75th – 25th and whiskers. For each parameter, the value corresponds to the following relationship: $\frac{AOD_{model} - AOD_{MODIS}}{AOD_{MODIS}}$ and statistical parameters (correlation coefficient R, normalized mean bias NMB, root mean square error RMSE, and normalized mean error NME) are calculated using monthly mean AODs over eastern China and northern India in August and September 2008.

Eastern China Models	mean (%)	median (%)	75th – 25th (%)	whiskers (%)	R	NMB (%)	RMSE	NME (%)
ECHAM6-HAM2	−47.9	−48.4	−37.2	−68.0	0.70	−36.0	0.21	38.9
EMEP	24.5	13.2	54.1	43.7	0.71	41.2	0.30	49.5
HadGEM	29.6	25.7	34.2	51.2	0.73	29.1	0.20	37.9
NorESM	−2.1	5.3	−3.8	−2.3	0.39	−1.9	0.20	37.7
OsloCTM2	−17.4	−20.7	−6.0	−25.8	0.63	−14.1	0.19	30.2
TM4-ECPL	−2.8	3.7	−6.1	−5.7	0.69	−2.0	0.15	25.9
WRF-Chem	−16.8	−20.4	5.8	−17.5	0.73	12.2	0.20	30.5
Model mean	−4.7	−4.1	−3.4	−5.6	0.82	4.1	0.12	20.8
Northern India Models	**mean (%)**	**median (%)**	**75th – 25th (%)**	**whiskers (%)**	R	**NMB (%)**	**RMSE**	**NME (%)**
ECHAM6-HAM2	−46.7	−47.4	−58.5	−63.2	0.62	−46.1	0.17	46.2
EMEP	−56.4	−68.9	−11.6	−59.0	0.56	−35.5	0.18	51.2
HadGEM	−2.9	3.0	11.9	2.6	0.78	24.8	0.13	32.6
NorESM	−36.8	−36.0	−78.7	−61.0	0.55	−23.9	0.13	33.2
OsloCTM2	13.2	−5.0	12.3	22.3	0.33	39.8	0.29	64.9
TM4-ECPL	−33.2	−32.7	−55.6	−47.6	0.72	−26.0	0.12	30.4
WRF-Chem	−17.5	−13.5	−7.0	−15.3	0.77	−2.1	0.10	26.0
Model mean	−25.8	−22.7	−43.0	−35.4	0.78	−9.9	0.08	21.9

ACPD
15, 11049–11109, 2015

Table 7. Correlation coefficient R, normalized mean bias NMB, root mean square error RMSE, and normalized mean error NME) calculated from monthly mean differences between MODIS and simulated AODs over the Asian domain for August and September 2008.

	Rest of the domain			
Models	R	NMB (%)	RMSE	NME (%)
ECHAM6-HAM2	0.66	−55.3	0.17	57.3
EMEP	0.70	−29.3	0.16	50.4
HadGEM	0.72	21.4	0.13	41.1
NorESM	0.62	−3.3	0.13	37.5
OsloCTM2	0.62	−31.1	0.15	43.5
TM4-ECPL	0.71	−0.49	0.12	32.6
WRF-Chem	0.63	−27.1	0.14	39.9
Model mean	0.78	−17.8	0.10	28.4

ACPD
15, 11049–11109, 2015

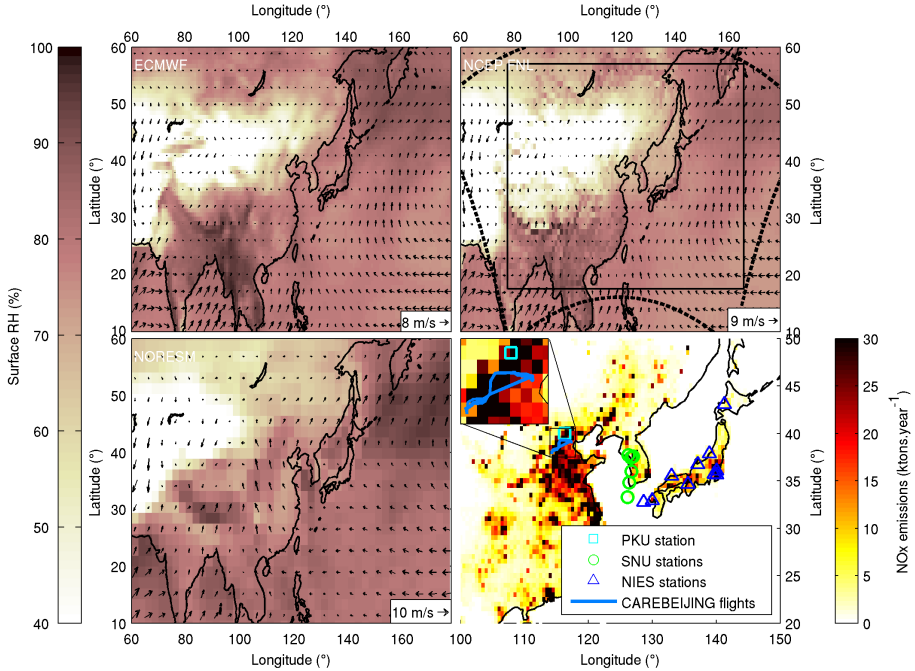

Figure 1. Map of the Asian region showing mean surface relative humidity (%) and surface wind speed ($m s^{-1}$) and direction (°) for August and September 2008 from ECMWF (top left panel), NCEP (National Centers for Environmental Prediction) FNL (final, top right panel), and NorESM (bottom left panel), and the NO_x emissions over east-Asia (bottom right panel). The WRF-Chem domain (dashed line) and the satellite data comparison domain (thick black line) are shown in the top right panel whereas the ground-based stations (cyan square, green circles, blue triangles), and the CAREBEIJING flight tracks (blue lines) used in this study are shown in the bottom right panel.

ACPD
15, 11049–11109, 2015

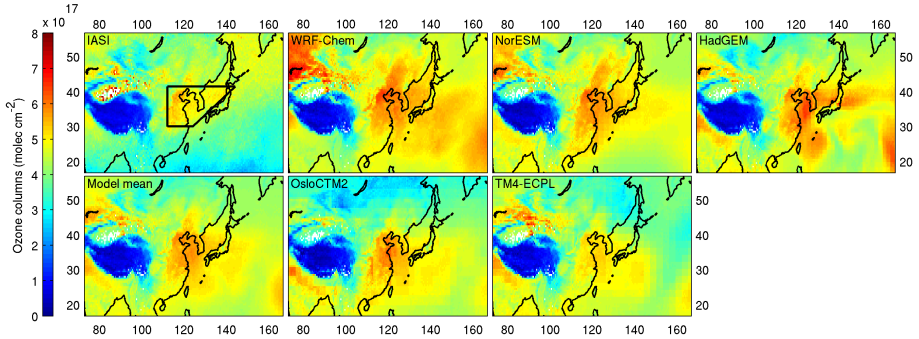

Figure 2. Average 0–6 km ozone columns (molec cm^{-2}) over Asia in August 2008 observed by the IASI satellite (left panel) and simulated by the models (models names are given in each relevant panel). The black polygon delimits the region discussed in detail in the text.

ACPD
15, 11049–11109, 2015

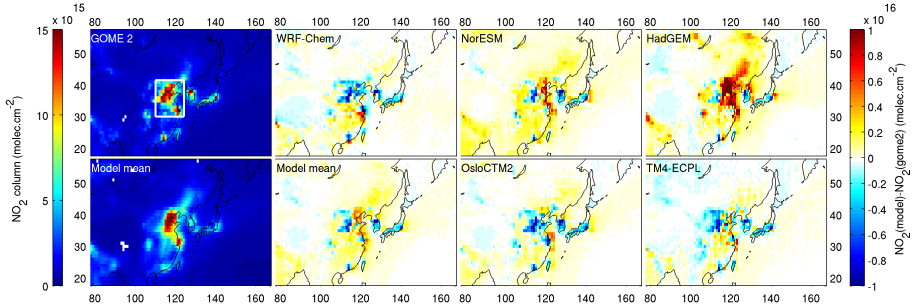

Figure 3. Mean tropospheric NO_2 columns in molec cm^{-2} (between the ground and the tropopause height given in the GOME-2 product) in August and September 2008 over Asia as observed by the GOME-2 satellite and absolute differences between GOME-2 and model simulations (model names are given in the panels). Model mean tropospheric columns are also presented in the bottom left panel. The white square denotes the emission region discussed in the text.

ACPD
15, 11049–11109, 2015

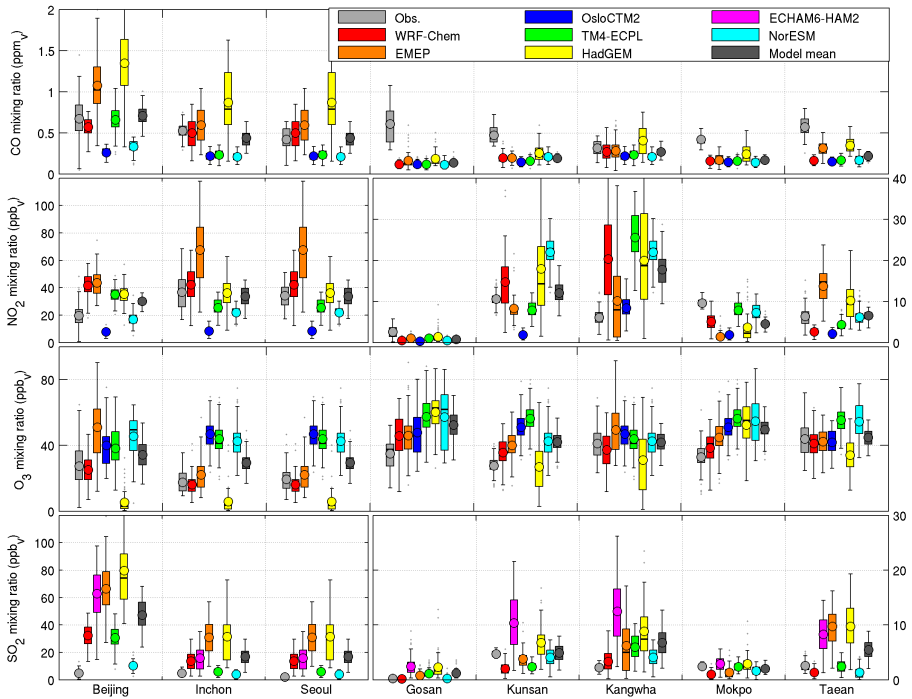

Figure 4. Box and whisker plots showing (from top to bottom) CO, NO_2, ozone, and SO_2 mean (circle), median (central line), 25th and 75th percentile (box edges) concentrations in volume mixing ratio (ppbv), during August and September 2008 as observed and simulated at eight surface sites in East Asia. The whiskers encompass values from 25th – 1.5 · (75th – 25th) to the 75th + 1.5 · (75th – 25th). This range covers more than 99 % of a normally distributed dataset. Note the different scales between urban (3 left) and rural (5 right) stations for NO_2 and SO_2 panels.

ACPD
15, 11049–11109, 2015

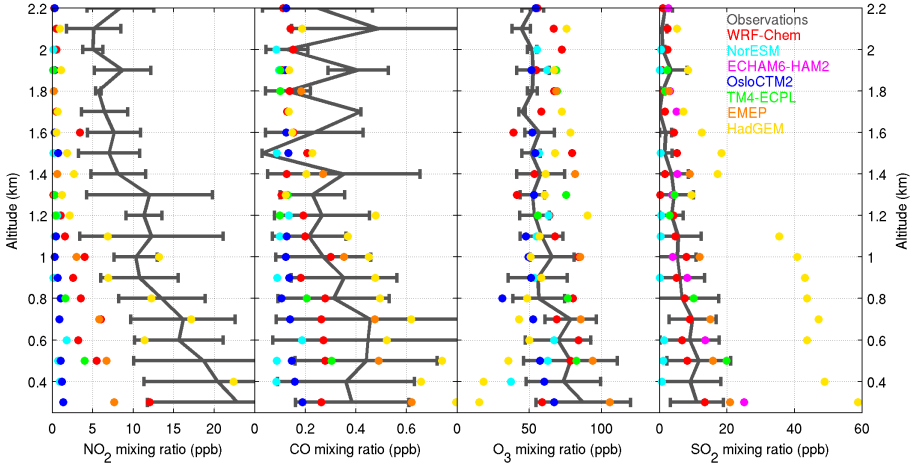

Figure 5. Mean vertical profiles of ozone, NO_2, CO, and SO_2 observed over China during the CAREBEIJING 2008 airborne campaign and simulated by the ECLIPSE models.

ACPD
15, 11049–11109, 2015

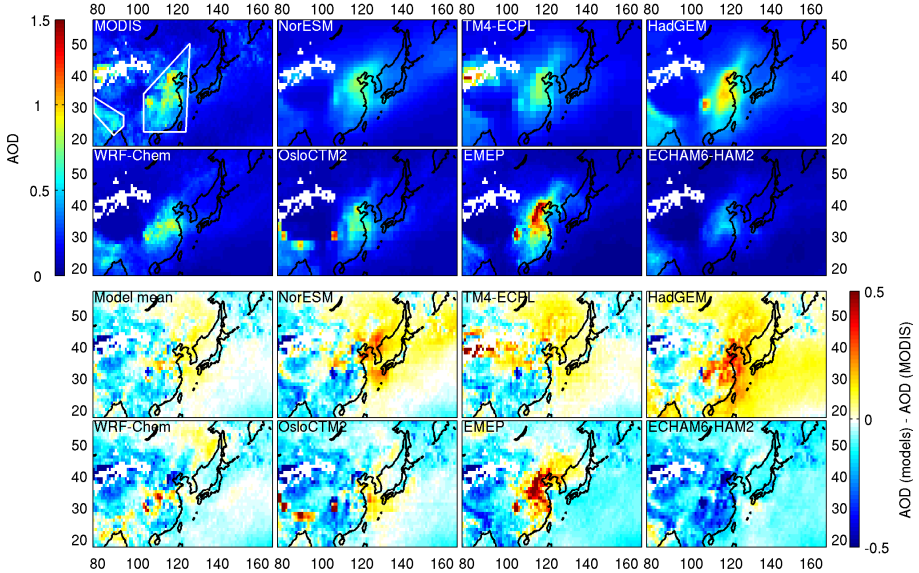

Figure 6. (8 top panels) Mean AODs observed by MODIS and simulated by the ECLIPSE models for August and September 2008, and (8 bottom panels) absolute differences between the simulated and the MODIS AODs (models names are given in each relevant panel). White polygons mark out the two regions discussed in the text.

ACPD
15, 11049–11109, 2015

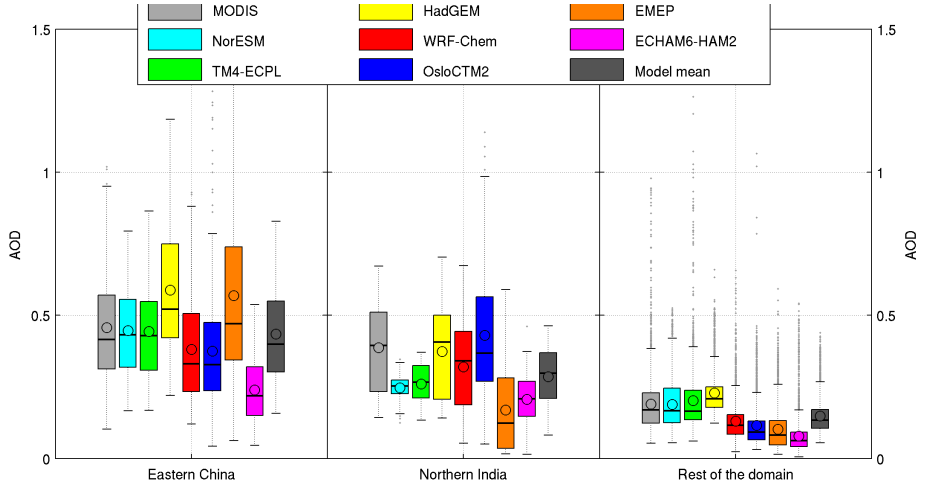

Figure 7. Box plots showing the mean AODs (circle), median (central line), 25th and 75th percentiles (box edges), and the extreme data not considered as outliers (whiskers) during August and September 2008 as observed by MODIS and simulated by the ECLIPSE models over northern India, eastern China and the rest of the domain.

ACPD
15, 11049–11109, 2015




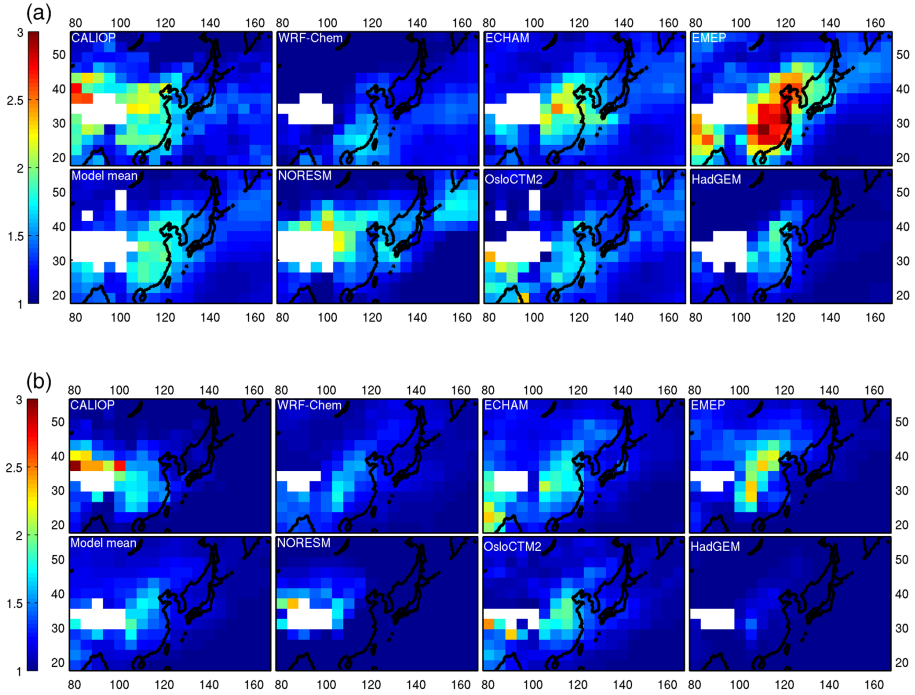

Figure 8. (a) Comparison between R_{app} over Asia in August and September 2008 averaged over a 0–2 km layer derived from CALIOP data and simulated by the ECLIPSE models. White boxes indicate missing observations due to ground elevation. **(b)** Comparison between R_{app} over Asia in August and September 2008 averaged over a 2–4 km layer derived from CALIOP data and simulated by the ECLIPSE models. White boxes indicate missing observations due to ground elevation.

ACPD
15, 11049–11109, 2015

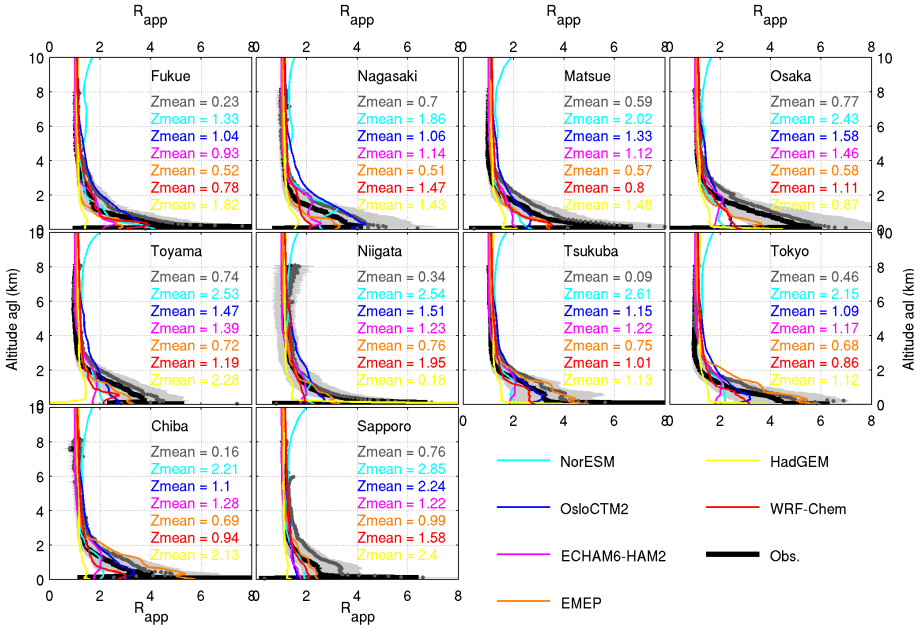

Figure 9. Comparison of mean (grey dots), median (black line), 25th and 75th percentiles (grey area) of R_{app} profiles observed at 10 NIES aerosol lidar stations over Japan (location shown in Fig. 1) and mean R_{app} (colored lines) simulated by the ECLIPSE models.

ACPD
15, 11049–11109, 2015

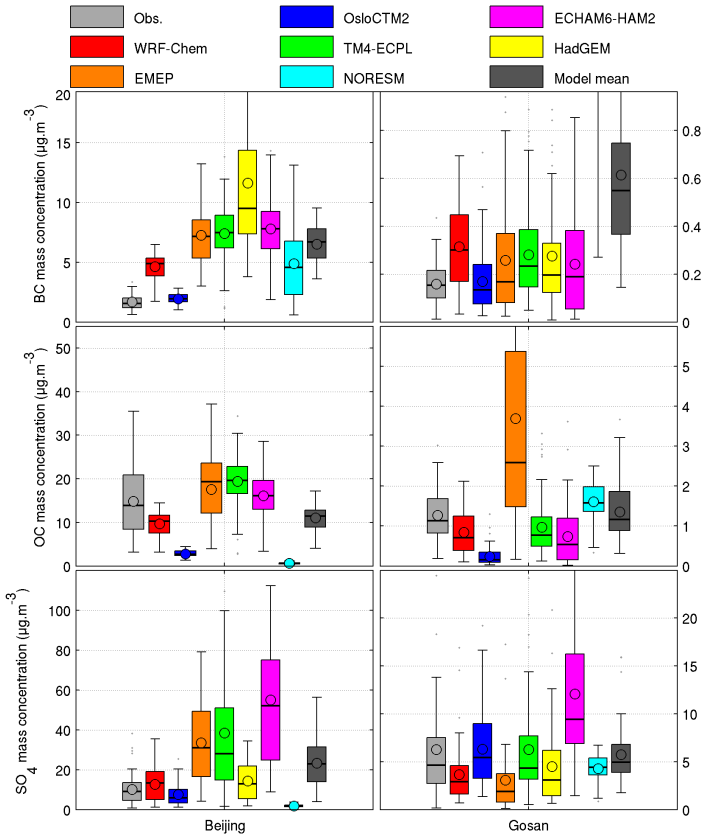

Figure 10. Comparison of observed and simulated box and whisker plots for BC, OC and sulphate: mean (circle), median (central line), 25th and 75th percentiles (box edges). The whiskers encompass values from 25th – 1.5·(75th – 25th) to the 75th + 1.5·(75th – 25th). This range covers more than 99 % of a normally distributed dataset. Note the different scales between urban and rural stations for NO_2 and SO_2 panels.

ACPD
15, 11049–11109, 2015